

EFFICIENT MONTE CARLO METHOD FOR INTEGRAL FRACTIONAL LAPLACIAN IN MULTIPLE DIMENSIONS *

CHANGTAO SHENG [†], BIHAO SU [†], AND CHENGLONG XU [†]

Abstract. In this paper, we develop a Monte Carlo method for solving PDEs involving an integral fractional Laplacian (IFL) in multiple dimensions. We first construct a new Feynman-Kac representation based on the Green function for the fractional Laplacian operator on the unit ball in arbitrary dimensions. Inspired by the “walk-on-spheres” algorithm proposed in [24], we extend our algorithm for solving fractional PDEs in the complex domain. Then, we can compute the expectation of a multi-dimensional random variable with a known density function to obtain the numerical solution efficiently. The proposed algorithm finds it remarkably efficient in solving fractional PDEs: it only needs to evaluate the integrals of expectation form over a series of inside ball tangent boundaries with the known Green function. Moreover, we carry out the error estimates of the proposed method for the n -dimensional unit ball. Finally, ample numerical results are presented to demonstrate the robustness and effectiveness of this approach for fractional PDEs in unit disk and complex domains, and even in ten-dimensional unit balls.

Key words. Integral fractional Laplacian, Green function, Monte Carlo method, Spherical coordinate

AMS subject classifications. 37P30, 60G22, 65C05, 65L70, 91G60

1. Introduction. Fractional powers of the Laplacian operator are a powerful tool in modeling phenomena in anomalous diffusion, which arise naturally in the α -stable Lévy process instead of the Brownian motion for normal diffusion (see, e.g., [7, 27, 28, 35] and the references therein). It is known that for $\alpha \in (0, 2)$, the fractional Laplacian of a sufficiently nice function $u(\mathbf{x}) : \mathbb{R}^n \rightarrow \mathbb{R}$ has the hypersingular integral representation (cf. [30]):

$$(1.1) \quad (-\Delta)^{\frac{\alpha}{2}} u(\mathbf{x}) = C_{n,\alpha} \text{p.v.} \int_{\mathbb{R}^n} \frac{u(\mathbf{x}) - u(\mathbf{y})}{|\mathbf{x} - \mathbf{y}|^{n+\alpha}} d\mathbf{y}, \quad C_{n,\alpha} := \frac{2^\alpha \Gamma(\frac{n+\alpha}{2})}{\pi^{\frac{n}{2}} \Gamma(1 - \frac{\alpha}{2})},$$

where “p.v.” stands for the principle value and $C_{n,\alpha}$ is the normalisation constant. This point-wise expression for the fractional Laplacian can directly be derived from the following Fourier transform:

$$(1.2) \quad (-\Delta)^{\frac{\alpha}{2}} u(\mathbf{x}) = \mathcal{F}^{-1} [|\boldsymbol{\xi}|^\alpha \mathcal{F}[u](\boldsymbol{\xi})](\mathbf{x}), \quad \mathbf{x} \in \mathbb{R}^n.$$

The nonlocal and singular nature of this operator poses major difficulties in discretisation and analysis. In the case where $\alpha = 2$ the operator coincides with the usual negative Laplacian $-\Delta$. Most recent concerns are with PDEs involving the IFL operator on an open bounded Lipschitz domain $\Omega \subset \mathbb{R}^n$. More precisely, given $f : \Omega \rightarrow \mathbb{R}$ in a suitable space, we look for u on Ω satisfying the fractional Poisson equation with the (nonlocal) Dirichlet boundary condition:

$$(1.3) \quad \begin{cases} (-\Delta)^{\frac{\alpha}{2}} u(\mathbf{x}) = f(\mathbf{x}), & \text{in } \Omega, \\ u(\mathbf{x}) = g(\mathbf{x}), & \text{on } \Omega^c := \mathbb{R}^n \setminus \Omega. \end{cases}$$

1.1. Review on existing studies. The numerical method for fractional Poisson equation (1.3) is challenging due to the nonlocality of the fractional Laplacian operator, hyper-singular integrals, and the low regularity of the solution at the boundary. In general, the existing approaches can be classified into the following two categories.

*Submitted to the editors DATE.

Funding: The research of the first author is partially supported by Shanghai Pujiang Program 21PJ1403500, the Fundamental Research Funds for the Central Universities 2021110474 and Shanghai Post-doctoral Excellence Program 2021154. The research of the third author is partially supported by the Fundamental Research Funds for the Central Universities.

[†]School of Mathematics, Shanghai University of Finance and Economics, Shanghai 200433, China. Email: ct-sheng@sufe.edu.cn (C. Sheng); subihao@163.sufe.edu.cn (B. Su); xu.chenglong@shufe.edu.cn (C. Xu).

The first is to discretize the fractional Poisson equations using deterministic numerical methods. It is customary to apply finite difference methods for integral fractional Laplacian (see, e.g., [14, 15, 23, 29] and many references therein). However, those finite difference discretizations are only available for simple domains such as rectangular domains and require stronger regularity assumptions for the solution. The finite element methods are more preferable for solving fractional PDEs, as it has a well-established theoretical foundation and the capability to deal with complex domain. The IFL operator has interwoven connections with the fractional Sobolev framework (cf. [30]), so the finite element scheme can be established under more realistic assumptions, i.e., in fractional Sobolev space and without additional regularity requirements. There have been many recent works devoted to the FEM analysis for fractional PDEs (see, e.g., [1, 2, 4–6, 17] and the references therein), but the literature on FEM implementation in multiple dimensions is very limited. Compared with the local schemes, the special designed spectral methods could compensate for the weakly singular behavior of the solution and hence are expected to approximate the solution of (1.3) accurately. However, the spectral methods are limited to one dimension, simple domains, and the whole space case, we refer to [10, 21, 22, 26, 34, 36] and the references therein for more details. Needless to say, for IFL on the bounded domain, these methods become complicated even for $n = 2, 3$ and computationally prohibitive for the higher-dimensional cases.

The second is to use Monte Carlo methods based on the stochastic processes to alleviate its proverbial numerical difficulties. It is well-known that the Feynman-Kac formula is an important bridge to link PDEs and stochastic processes (see, e.g., [11, 12, 18, 24, 38] and the references therein), which offers a method of solving certain PDEs via simulating random paths of a stochastic process. For the classical Poisson equations, that is,

$$(1.4) \quad -\Delta u(\mathbf{x}) = f(\mathbf{x}) \quad \text{in } \Omega; \quad u(\mathbf{x}) = g(\mathbf{x}) \quad \text{on } \partial\Omega,$$

which is governed by Brownian motion and the solution (1.4) has a Feynman-Kac representation, expressed as an expectation at first exit from Ω of the associated Wiener process (cf. [13]). Remarkably, in [13, 24], the Feynman-Kac representation was extended to fractional Laplacian, where Brownian motion was replaced by α -stable Lévy process. Let $\Omega \subset \mathbb{R}^n$ be a bounded domain, with $n \geq 1$. For any $\alpha \in (0, 2)$ and a Borel set $\Lambda \subset \mathbb{R}^n$, we denote

$$L_\alpha^1(\Lambda) = \left\{ u \in L^1(\Lambda) \text{ s.t. } \int_\Lambda \frac{|u(x)|}{1 + |x|^{n+\alpha}} dx < \infty \right\}.$$

Suppose that $g(x)$ is a continuous function that belongs to $L_\alpha^1(\Omega^c)$, and $f(x)$ is a function in $C^{\alpha+\epsilon}(\Omega)$ for some $\epsilon > 0$. Then there exists a unique continuous solution to problem (1.3) in $L_\alpha^1(\mathbb{R}^n)$, which is given by (see [24, Thm. 6.1])

$$(1.5) \quad u(x) = \mathbb{E}_{X_0^\alpha=x}[g(X_{\tau_\Omega}^\alpha)] + \mathbb{E}_{X_0^\alpha=x}\left[\int_0^{\tau_\Omega} f(X_s^\alpha) ds\right], \quad x \in \Omega,$$

where $\tau_\Omega = \inf\{t > 0 : X_t^\alpha \notin \Omega\}$, and $\{X_t^\alpha\}_{t \geq 0}$ is a symmetric α -stable Lévy process with $X_0^\alpha = x$. We recall that a stochastic process $\{X_t^\alpha; t \geq 0\}$ is called symmetric α -stable Lévy process if:

- (1). $X_0^\alpha = 0$ a.s.;
- (2). X_t^α has independent and stationary increments;
- (3). $X_t^\alpha - X_s^\alpha \sim S_\alpha((t-s)^{1/\alpha}, 0, 0)$ for any $0 \leq s < t < \infty$, that is, α -stable distribution with scale parameter $(t-s)^{1/\alpha}$, and skewness and shift parameters equal to zero.

In particular, when $\alpha = 2$, then $X_t^2 = \sqrt{2}B_t$, B_t represents the standard Brownian motion. The symmetric α -stable Lévy process is $1/\alpha$ self-similar. That is for $k > 0$, the process $\{X_{kt}^\alpha; t \geq 0\}$ and $\{k^{1/\alpha}X_t^\alpha; t \geq 0\}$ have the same finite-dimensional distributions. The characteristic function

(see [3]) of a α -stable random variable X is given by

$$(1.6) \quad \ln \psi(\theta) = \begin{cases} -\sigma^\alpha |\theta|^\alpha [1 - i\beta \operatorname{sgn}(\theta) \tan(\frac{\alpha\pi}{2}) + i\mu\theta], & \text{if } \alpha \in (0, 1) \cup (1, 2], \\ -\sigma |\theta| [1 + i\beta \frac{2}{\pi} \operatorname{sgn}(\theta) \ln |\theta| + i\mu\theta], & \text{if } \alpha = 1, \end{cases}$$

where $\alpha \in (0, 2]$ is the index of stability, $\beta \in [-1, 1]$ denotes the skewness parameter, $\mu \in \mathbb{R}$ and $\sigma > 0$ represent the shift and scale parameters respectively. Then X is called α -random variable, and we use the notation $X \sim S_\alpha(\sigma, \beta, \mu)$. Obviously, $S_1(\sigma, 0, \mu)$ and $S_2(\sigma, 0, \mu)$ are the Cauchy distribution and the Gaussian distribution $\mathcal{N}(\mu, \sigma)$, respectively (cf. [3]).

This groundbreaking representation provides a viable alternative for its mathematical and numerical treatment. Kyprianou et al. [24] developed an efficient Monte Carlo method for (1.3) in two dimensions by using the walk-on-spheres algorithm, which is based on the Feynman-Kac representation. With this idea, Shardlow [33] proposed the multilevel Monte Carlo method combined with the Walk outside spheres algorithm for solving the eigenvalues problem involving fractional Laplacian operator. Those methods can be extended to high-dimensional cases. However, it will become complicated, as the Feynman-Kac representation is associated with a high dimensional α -stable process, which seems not an easy task. Thus, extending those approaches to a higher dimensional case is nontrivial.

We also remark that direct learning of the IFL and/or nonlocal models on bounded domains was discussed in some recent works (see, e.g., [9, 31] for Physical-informed neural networks (PINN); and [19, 20, 25, 32, 37] for deep learning methods). We note that most current works tend to combine the traditional automatic differential method with some typical numerical discretization to solve the fractional or nonlocal models.

1.2. Our contributions and the organization of the paper. This paper proposes and analyzes a Monte Carlo method for PDEs involving integral fractional Laplacian on the bounded domain in arbitrary dimensions. The proposed method takes advantage of the Feynman-Kac representation based on Green functions for the simulation of both classical and fractional Laplacians in a unified framework, which avoids the enormous computational cost of evaluating the fractional derivatives. We highlight below the main advantages of the proposed methods and main contributions of the paper:

- We provide a new Feynman-Kac representation for the solution of fractional Poisson equations on the ball in arbitrary dimensions (see Lemma 2.3 below). Benefiting from the new representation, to avoid calculating the expectation of a complex integral that involves the function of α -stable Lévy process, we can evaluate the expectation of a random variable associated with the explicit expression of the Green functions to obtain the solution.
- We further extended the representation for fractional PDEs on the irregular domain. More precisely, as shown in Theorem 2.5 of this paper, the solution of (1.3) on an open bounded domain can be evaluated by the expectation of a sequence of inside balls tangent to the boundary, as the Green's function and Poisson's kernel on the balls are known. The existing work [24] is to adopt the walk-on-spheres algorithm for solving fractional Poisson equation in two dimensions, in which the walk-on-spheres process is associated with the α -stable process.
- The proposed method is capable of fractional PDEs in high dimensions. Moreover, in the Monte Carlo procedure, thanks to spherical coordinates, the distribution in the angular direction for each jump is uniform, allowing us only need to appropriately increase the samples in the angular direction with the increase of dimensionality so that the computation time will increase at a moderate pace.
- We fully analyze the error analysis and characterize the efficiency of the proposed method for fractional Poisson equations on the ball in arbitrary dimensions, with the aid of the property of the Monte Carlo procedure and the explicit expressions of the Green functions.

The rest of the paper is organized as follows. In the next section, we derive an alternative formula based on the Green function of integral fractional Laplacian operator on the unit ball in arbitrary dimensions and extend the result to the case of irregular domain. Section 3 describes the detailed algorithm for computing the fractional PDEs based on the Monte Carlo method. In Section 4, we provide a complete error analysis of the proposed methods for the fractional Poisson equation. Numerical experiments for PDEs with integral fractional Laplacian are carried out in Section 5. Some concluding remarks are given in the last section.

2. Main results.

2.1. Feynman-Kac representation in expectation form in a ball. In this section, we introduce some representation formula for the solution of fractional Laplacian operator on the ball in arbitrary dimensions. To this ends, we set $\mathbf{c}_0 \in \mathbb{R}^n$ and define $r > 0$ to be the radius of a ball inscribed in \mathbb{R}^n that is centered at \mathbf{c}_0 . This sphere we will call $\mathbb{B}_r^{n, \mathbf{c}_0} = \{\mathbf{x} \in \mathbb{R}^n : |\mathbf{x} - \mathbf{c}_0| \leq r\}$. Let $\mathbb{B}_r^n = \mathbb{B}_r^{n, \mathbf{0}}$ for simplicity.

We first show that the solution of (1.3) on the ball can be explicitly represented as the following integral form as follows, which play important role in the algorithm development.

LEMMA 2.1. *Let $r > 0$ and $\alpha \in (0, 2]$. If $f \in L_\alpha^1(\mathbb{B}_r^n) \cap C(\overline{\mathbb{B}_r^n})$, $g \in L_\alpha^1(\mathbb{R}^n \setminus \mathbb{B}_r^n)$, then the solution of (1.3) with $\Omega = \mathbb{B}_r^n$ can be represented as*

$$(2.1) \quad u(\mathbf{x}) = \begin{cases} \int_{\mathbb{B}_r^n} f(\mathbf{y}) Q_r(\mathbf{x}, \mathbf{y}) d\mathbf{y} + \int_{\mathbb{R}^n \setminus \mathbb{B}_r^n} g(\mathbf{z}) P_r(\mathbf{x}, \mathbf{z}) d\mathbf{z}, & \text{in } \mathbb{B}_r^n, \\ g(\mathbf{x}), & \text{on } \mathbb{R}^n \setminus \mathbb{B}_r^n, \end{cases}$$

where $P_r(\mathbf{x}, \mathbf{z})$ is the Poisson kernel defined by

$$(2.2) \quad P_r(\mathbf{x}, \mathbf{z}) = \tilde{C}_n^\alpha \left(\frac{r^2 - |\mathbf{x}|^2}{|\mathbf{z}|^2 - r^2} \right)^{\alpha/2} \frac{1}{|\mathbf{x} - \mathbf{z}|^n}, \quad \mathbf{x} \in \mathbb{B}_r^n, \quad \mathbf{z} \in \mathbb{R}^n \setminus \overline{\mathbb{B}_r^n},$$

and for $\mathbf{x} \neq \mathbf{y}$,

$$(2.3) \quad Q_r(\mathbf{x}, \mathbf{y}) = \begin{cases} \hat{C}_n^\alpha |\mathbf{y} - \mathbf{x}|^{\alpha-n} \int_0^{\varrho(\mathbf{x}, \mathbf{y})} \frac{t^{\frac{\alpha}{2}-1}}{(t+1)^{\frac{n}{2}}} dt, & \alpha \neq n, \\ \hat{C}_1^{\frac{1}{2}} \log \left(\frac{r^2 - \mathbf{x}\mathbf{y} + \sqrt{(r^2 - \mathbf{x}^2)(r^2 - \mathbf{y}^2)}}{r|\mathbf{y} - \mathbf{x}|} \right), & \alpha = n, \end{cases}$$

with

$$(2.4) \quad \varrho(\mathbf{x}, \mathbf{y}) = \frac{(r^2 - |\mathbf{x}|^2)(r^2 - |\mathbf{y}|^2)}{r^2 |\mathbf{x} - \mathbf{y}|^2}.$$

In the above, the constants

$$(2.5) \quad \tilde{C}_n^\alpha = \frac{\Gamma(n/2) \sin(\pi\alpha/2)}{\pi^{\frac{n}{2}+1}}, \quad \hat{C}_n^\alpha = \frac{\Gamma(n/2)}{2^\alpha \pi^{\frac{n}{2}} \Gamma^2(\alpha/2)}.$$

Remark 2.2. *Note that if $\alpha = 2$, the stochastic process is the standard Brownian motion, and the corresponding Green's function and Poisson's kernel are given by*

$$Q_r(\mathbf{x}, \mathbf{y}) = -\frac{1}{2\pi} \log \frac{1}{|\mathbf{y} - \mathbf{x}|}, \quad P_r(\mathbf{x}, \mathbf{z}) = \frac{1}{2\pi r} \frac{r^2 - |\mathbf{x}|^2}{|\mathbf{x} - \mathbf{z}|^2}, \quad \text{if } n = 2.$$

If $\alpha = 2$ and $n = 3$, there holds

$$Q_r(\mathbf{x}, \mathbf{y}) = -\frac{1}{4\pi} \left[\frac{1}{|\mathbf{y} - \mathbf{x}|} - \frac{1}{\sqrt{|\mathbf{y}|^2 + |\mathbf{x}|^2 - 2\mathbf{x}\mathbf{y} \cos \theta} - \sqrt{r^2 + \frac{|\mathbf{x}|^2 |\mathbf{y}|^2}{r^2} - 2\mathbf{x}\mathbf{y} \cos \theta}} \right],$$

$$P_r(\mathbf{x}, \mathbf{z}) = \frac{1}{4\pi r} \frac{r^2 - |\mathbf{x}|^2}{|\mathbf{x} - \mathbf{z}|^3}.$$

where θ represents the angle between the vectors \mathbf{x} and \mathbf{y} .

The following alternative formulation with explicit expression for the solution of (1.3) is more convenient for computation, where we transform the expression of the original solution (2.1) into an expectation form.

LEMMA 2.3. *Let $\Omega = \mathbb{B}_r^n$ with $r > 0$, and assume that $f \in L^1_\alpha(\mathbb{B}_r^n) \cap C(\overline{\mathbb{B}_r^n})$ and $g \in L^1_\alpha(\mathbb{R}^n \setminus \mathbb{B}_r^n)$, then the solution of problem (1.3) in $L^1_\alpha(\mathbb{R}^n)$ can also be expressed as*

$$(2.6) \quad u(\mathbf{x}) = \zeta(\mathbf{x}) \mathbb{E}_{\tilde{Q}_r} [f(Y)] + \mathbb{E}_{P_r} [g(Z)], \quad Y \in \mathbb{B}_r^n, Z \in \mathbb{R}^n \setminus \mathbb{B}_r^n,$$

where $\zeta(\mathbf{x})$ is the weight function of the form

$$(2.7) \quad \zeta(\mathbf{x}) = \int_{\mathbb{B}_r^n} Q_r(\mathbf{x}, \mathbf{y}) d\mathbf{y}.$$

In the above, the first term represents a weighted average of the source f inside the ball, and the second term denotes a mean value with respect to the function P_r outside the ball.

Proof. To obtain probability density function for $f(x)$, we normalize the Green function as

$$(2.8) \quad \tilde{Q}_r(\mathbf{x}, \mathbf{y}) = \frac{Q_r(\mathbf{x}, \mathbf{y})}{\zeta(\mathbf{x})},$$

where $\zeta(x)$ is defined in (2.7). According to [8, Lemma A.5], we have

$$(2.9) \quad \int_{\mathbb{R}^n \setminus \mathbb{B}_r^n} P_r(\mathbf{x}, \mathbf{z}) d\mathbf{z} = 1,$$

which implies $P_r(\mathbf{x}, \mathbf{z})$ is probability density function for $g(\mathbf{z})$. Thus, we have

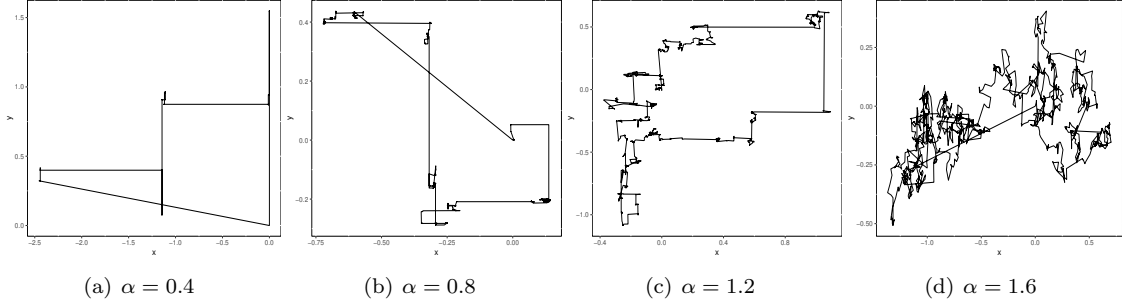
$$(2.10) \quad \begin{aligned} u(\mathbf{x}) &= \int_{\mathbb{B}_r^n} f(\mathbf{y}) Q_r(\mathbf{x}, \mathbf{y}) d\mathbf{y} + \int_{\mathbb{R}^n \setminus \mathbb{B}_r^n} g(\mathbf{z}) P_r(\mathbf{x}, \mathbf{z}) d\mathbf{z} \\ &= \zeta(\mathbf{x}) \int_{\mathbb{B}_r^n} f(\mathbf{y}) \tilde{Q}_r(\mathbf{x}, \mathbf{y}) d\mathbf{y} + \int_{\mathbb{R}^n \setminus \mathbb{B}_r^n} g(\mathbf{z}) P_r(\mathbf{x}, \mathbf{z}) d\mathbf{z} = \zeta(\mathbf{x}) \mathbb{E}_{\mathbf{x}} [f(Y)] + \mathbb{E}_{\mathbf{x}} [g(Z)]. \end{aligned}$$

This completes the proof. \square

Remark 2.4. It should be pointed out that both (1.5) and (2.6) can be used to construct the Monte Carlo method for solving (1.3) on \mathbb{B}_r^n . The main difference is the corresponding stochastic process of (1.5) is associated with α -stable Lévy process. While (2.6) can simplify the evaluation of each jump significantly with the aid of the explicit expression of Green function \tilde{Q}_r and Poisson kernel P_r (see (2.2) and (2.3)).

2.2. A new representation in expectation form for the irregular domain. This section will focus on the expressions for the solutions of PDEs involving IFL (1.3) on the irregular domain in arbitrary dimensions. Although it is difficult to find the Green function \tilde{Q}_r and Poisson kernel P_r on the irregular domain Ω , the fractional Poisson equation on the irregular domain can be approximated by the whole motion path with a sequence of small ball. According to (1.5), we know that the solution of (1.3) on any irregular domain can be simulated via an α -stable process (cf. Fig. 1), and this process stops when it reaches the outside of the region. Recall that the solution of (1.3) corresponds to α -stable process X_t^α and can be rewritten in the form of path integral as (cf. [24])

$$u(\mathbf{x}) = \mathbb{E}_{X_0^\alpha = \mathbf{x}} \left[\int_0^{\tau_\Omega} f(X_s^\alpha) ds \right] + \mathbb{E}_{X_0^\alpha = \mathbf{x}} [g(X_{\tau_\Omega}^\alpha)], \quad \mathbf{x} \in \Omega,$$

FIG. 1. The motion trajectory of α -stable process.

where τ_Ω is the first passage time and $X_{\tau_\Omega}^\alpha$ is the first passage location on the region $\mathbb{R}^n \setminus \Omega$, and $\mathbb{E}_x[\tau_\Omega] < \infty$, for all $x \in \Omega$.

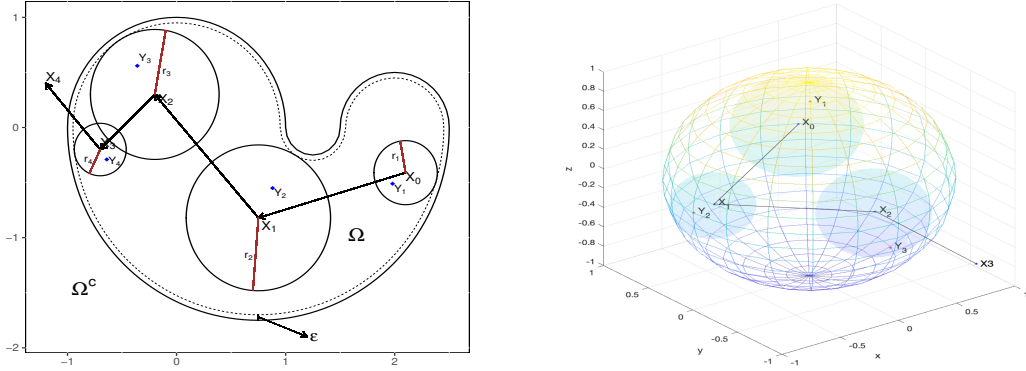


FIG. 2. The path of walk; Left: on 2-D irregular domain; Right: on the unit ball in 3-D.

Since the Markov process will leave the given domain at a finite time, the discrete point sequence can reach outside the domain Ω after a limited number of steps. Therefore, at each jump, the probability of this point leaving the given region at the next move always be positive, that is, $P(m^* < \infty) = 1$, where we denoted by

$$(2.11) \quad m^* = \inf\{m : X_m \notin \Omega\},$$

the stopping step for the random walk. Hence, the Monte Carlo method can be use to calculate the existing observation paths, to obtain the value of $u(x)$, see Fig. 2.

THEOREM 2.5. *Let $\alpha \in (0, 2]$ and Ω be an open bounded domain, and assume that $f \in L_\alpha^1(\Omega) \cap C(\bar{\Omega})$ and $g \in L_\alpha^1(\mathbb{R}^n \setminus \Omega)$, then the solution of (1.3) in $L_\alpha^1(\mathbb{R}^n)$ can be expressed as*

$$(2.12) \quad u(x) = \sum_{k=1}^{m^*-1} \zeta(X_k) \mathbb{E}_{\bar{Q}_{r_k}}[f(Y_k)] + \mathbb{E}_{P_{r_{m^*-1}}}[g(Z_{m^*})], \quad Y_k \in \mathbb{B}_{r_k}, \quad Z_k \in \mathbb{R}^n \setminus \mathbb{B}_{r_k},$$

where $\zeta(X_k)$ is the weight function in k -th ball,

$$(2.13) \quad \zeta(X_k) = \int_{\mathbb{B}_{r_k}^n} Q_{r_k}(X_k, \mathbf{y}) \, d\mathbf{y}.$$

In the above, the first expectation represents the contribution of source f in k -th inside ball associated with the Green's function Q_{r_k} , and the second one describes a mean value of g outside the last ball $\mathbb{B}_{r_{m^*-1}}^n$ associated with $P_{r_{m^*-1}}$.

Proof. The α -stable process X_t^α can be surrounded by a series of small balls tangent to region Ω , that is, we can split the process X_t^α according to the time of movement within the region Ω . Let $0 = \tau_0 < \tau_1 < \tau_2 < \dots < \tau_{m^*} = \tau_\Omega$, τ_k ($0 < k < m^*$) denotes the time of movement away from the k -th ball. In view of (1.5), the solution of (1.3) have the following form

$$\begin{aligned} u(\mathbf{x}) &= \mathbb{E}_{X_0^\alpha = \mathbf{x}} \left[\int_0^{\tau_\Omega} f(X_s^\alpha) ds \right] + \mathbb{E}_{X_0^\alpha = \mathbf{x}} [g(X_{\tau_\Omega}^\alpha)] \\ &= \mathbb{E}_{X_0^\alpha = \mathbf{x}} \left[\int_{\tau_0}^{\tau_1} f(X_s^\alpha) ds + \int_{\tau_1}^{\tau_2} f(X_s^\alpha) ds + \dots + \int_{\tau_{m^*-1}}^{\tau_{m^*}} f(X_s^\alpha) ds \right] + \mathbb{E}_{X_0^\alpha = \mathbf{x}} [g(X_{\tau_\Omega}^\alpha)] \\ &= \mathbb{E}_{X_0^\alpha = \mathbf{x}} \left[\sum_{k=0}^{m^*-1} \int_{\tau_k}^{\tau_{k+1}} f(X_s^\alpha) ds \right] + \mathbb{E}_{X_0^\alpha = \mathbf{x}} [g(X_{\tau_{m^*}}^\alpha)]. \end{aligned}$$

As a result, a similar procedure as in Lemma 2.3 can be applied to each step of the above process. It is clear that each expectation, i.e., $\mathbb{E}_{X_0^\alpha = \mathbf{x}, X_{\tau_k}^\alpha = X_k} \left[\int_{\tau_k}^{\tau_{k+1}} f(X_s^\alpha) ds \right]$ can be view as the stochastic solution of the following fractional PDEs with homogeneous boundary condition

$$\begin{cases} (-\Delta)^{\frac{\alpha}{2}} u(\mathbf{x}) = f(\mathbf{x}), & \text{in } \mathbb{B}_{r_k}^n, \\ u(\mathbf{x}) = 0, & \text{on } \mathbb{R}^n \setminus \mathbb{B}_{r_k}^n. \end{cases}$$

Moreover, in the last step, the term $\mathbb{E}_{X_0^\alpha = \mathbf{x}, X_{\tau_{m^*-1}}^\alpha = X_{m^*-1}} \left[\int_{\tau_{m^*-1}}^{\tau_{m^*}} f(X_s^\alpha) ds \right] + \mathbb{E}_{X_0^\alpha = \mathbf{x}} [g(X_{\tau_{m^*}}^\alpha)]$ represents the stochastic solution of the following problem

$$\begin{cases} (-\Delta)^{\frac{\alpha}{2}} u(\mathbf{x}) = f(\mathbf{x}), & \text{in } \mathbb{B}_{r_{m^*-1}}^n, \\ u(\mathbf{x}) = g(\mathbf{x}), & \text{on } \mathbb{R}^n \setminus \mathbb{B}_{r_{m^*-1}}^n. \end{cases}$$

Then, we derive from (2.1) and (2.6) that

$$\begin{aligned} \mathbb{E}_{X_0^\alpha = \mathbf{x}} \left[\int_{\tau_k}^{\tau_{k+1}} f(X_s^\alpha) ds \right] &= \int_{\mathbb{B}_{r_k}^n} f(\mathbf{y}) Q_{r_k}(X_k, \mathbf{y}) d\mathbf{y} = \zeta(X_k) \int_{\mathbb{B}_{r_k}^n} f(\mathbf{y}) \tilde{Q}_{r_k}(X_k, \mathbf{y}) d\mathbf{y} \\ &= \zeta(X_k) \mathbb{E}_{\tilde{Q}_{r_k}} [f(Y_k)]. \end{aligned}$$

Since τ_{m^*} denotes the time for the process X_t^α to leave the $(m^* - 1)$ -th ball, and also leave domain Ω , then

$$\mathbb{E}_{X_0^\alpha = \mathbf{x}} [g(X_{\tau_{m^*}}^\alpha)] = \mathbb{E}_{P_{r_{m^*-1}}} [g(Z_{m^*})].$$

Consequently, a combination of the above results lead to the desired result. \square

2.3. Efficient algorithm. This section describe the Monto Carlo method using Green function and the representation (2.6) and (2.12) to solve the fractional PDEs on bounded domain. To fix the idea, we only consider the algorithm based on the representation (2.12), as (2.6) is a special case of (2.12).

Instead of simulating the irregular trajectories of symmetric α -stable processes, we take advantage of the explicit expressions of \tilde{Q}_r and P_r as the probability density functions, which gives the transition probability of the symmetric α -stable process trajectory inside the ball during its passage from the center to the boundary $\partial\Omega$ or outside the domain Ω (cf. Fig. 2). More precisely,

the representation (2.12) allows us to construct a sequence of inside balls $\{\mathbb{B}_{r_i}^n := \mathbb{B}_{r_i}^{n, \mathbf{x}_i}\}_{i \geq 0}$ tangent to the boundary $\partial\Omega$. In each ball, we construct a random variable whose value is only obtained inside the corresponding ball. The expected value of the symmetric α -stable process integral is replaced by the weighted expected value of this set of random variables. The centers of these balls are generated by a series of discrete transitions in continuous space \mathbb{R}^n that eventually terminate when they first reach the outside of domain Ω .

We denote by X_i the i -th random variable, and then generate the corresponding inside ball centered at X_i tangent the boundary $\partial\Omega$, i.e., $\mathbb{B}_{r_i}^{n, X_i}$. It is evident that the closer X_i approaches to the center of Ω , the bigger area of the ball will be. In other words, the area $\Omega \setminus \mathbb{B}_{r_i}^{n, X_i}$ will decrease as it moves away from the center. One verifies readily that the next time the ball moves, the less likely it is to be in $\Omega \setminus \mathbb{B}_{r_i}^{n, X_i}$. Conversely, when the center of the current ball is near $\partial\Omega$, the probability that the ball will be in $\Omega \setminus \mathbb{B}_{r_i}^{n, X_i}$ on its next move increases. Given an accuracy threshold $\varepsilon > 0$, we define an inwardly ‘thickening’ the boundary $\partial\Omega$ as (see Fig. 2 (left)):

$$(2.14) \quad \Gamma_\varepsilon = \{\mathbf{x} \in \Omega : \text{dist}(\mathbf{x}, \partial\Omega) < \varepsilon\},$$

where $\text{dist}(\mathbf{x}, \partial\Omega)$ denotes the distance from $\mathbf{x} \in \Omega$ to $\partial\Omega$. Therefore, to reduce the calculation, we assume that the Moto Carlo process stops when it reaches $\Gamma_\varepsilon \cup \Omega^c$. When ε is small enough if the ball moves into this domain Γ_ε , it’s considered outside the domain Ω .

Therefore, in each experiment, we need to simulate several important quantities as below

- (i). The coordinates of the center of i -th ball;
- (ii). The radius of the ball r_i , which is the distance in each discrete jump;
- (iii). The weight of the expectation $\zeta(\mathbf{x}_i)$;
- (iv). The expectation of the random variable in each ball $\mathbb{E}[f(Y)]$.

Dealing with the above quantities in high dimensional Cartesian coordinates appears difficult, therefore, to simplify the implementation, we recommend proceeding with this calculation in spherical coordinates. To this end, we denoted by $\hat{\mathbf{x}} = \mathbf{x}/|\mathbf{x}|$ the unit vector along the nonzero vector \mathbf{x} . We now recall the d -dimensional spherical coordinates

$$(2.15) \quad \begin{aligned} x_1 &= \rho \cos \theta_1; \quad x_2 = \rho \sin \theta_1 \cos \theta_2; \quad \cdots \cdots \cdots; \quad x_{n-1} = \rho \sin \theta_1 \cdots \sin \theta_{n-2} \cos \theta_{n-1}; \\ x_n &= \rho \sin \theta_1 \cdots \sin \theta_{n-2} \sin \theta_{n-1}, \quad \theta_1, \cdots, \theta_{n-2} \in [0, \pi], \quad \theta_{n-1} \in [0, 2\pi], \end{aligned}$$

with the spherical volume element

$$(2.16) \quad d\mathbf{x} = \rho^{n-1} \sin^{n-2} \theta_1 \sin^{n-3} \theta_2 \cdots \sin \theta_{n-2} d\rho d\theta_1 d\theta_2 \cdots d\theta_{n-1}.$$

2.3.1. Computation of the jump distance and weight function $\zeta(x)$. We can evaluate the jump distance (denoted by γ) from the current ball to the next ball by using the following formula, which indicates the jump distance is a uniformly distributed random number.

LEMMA 2.6. *Let $\alpha \in (0, 2]$ and let the radius of the current ball $r > 0$. Assume that the ball jumps in the region Ω , then the jump distance γ from the current ball to the next ball is given by*

$$(2.17) \quad \gamma(\omega; r, n, \alpha) = \sqrt{\frac{r^2}{B(1 - \frac{\alpha}{2}, \frac{\alpha}{2}) - B^{-1}(\frac{\pi\omega}{\sin(\pi\alpha/2)}; 1 - \frac{\alpha}{2}, \frac{\alpha}{2})}}, \quad \omega \in (0, 1),$$

where $B^{-1}(\cdot; a, b)$ denote the inverse function of incomplete Beta function $B(\cdot; a, b)$, and $B(a, b) := B(1; a, b)$ denote the Beta function.

Proof. Let $\mathbf{x} = |\mathbf{x}|e_n$, then we have $|\mathbf{x} - \mathbf{z}|^2 = |\mathbf{x}|^2 + |\mathbf{z}|^2 - 2|\mathbf{x}||\mathbf{z}| \cos \theta = \rho^2 + |\mathbf{z}|^2 - 2|\mathbf{x}|\rho \cos \theta$ (see Fig. 3). For $|\mathbf{z}| > r$ and $\mathbf{x} \neq \mathbf{0}$, we find from (2.2) and the above identity that

$$\int_{r < |\mathbf{z}| < \gamma} P_r(\mathbf{x}, \mathbf{z}) d\mathbf{z}$$

$$\begin{aligned}
 (2.18) \quad &= 2\pi \tilde{C}_n^\alpha (r^2 - |\mathbf{x}|^2)^{\frac{\alpha}{2}} \prod_{k=1}^{n-3} \int_0^\pi \sin^k \theta d\theta \int_r^\gamma \int_0^\pi \frac{\rho^{n-1} \sin^{n-2} \theta}{(\rho^2 - r^2)^{\alpha/2} (\rho^2 + |\mathbf{x}|^2 - 2\rho|\mathbf{x}| \cos \theta)^{n/2}} d\theta d\rho \\
 &= 2\pi \tilde{C}_n^\alpha (\bar{r}^2 - 1)^{\frac{\alpha}{2}} \prod_{k=1}^{n-3} \int_0^\pi \sin^k \theta d\theta \int_r^\gamma \frac{\bar{\rho}^{n-1}}{(\bar{\rho}^2 - r^2)^{\alpha/2}} \lambda(\bar{\rho}) d\bar{\rho},
 \end{aligned}$$

where we used $\bar{r} = r/|\mathbf{x}| > 1$, $\bar{\rho} = \rho/|\mathbf{x}| > 1$ in the last identity, and denoted

$$\lambda(\bar{\rho}) = \int_0^\pi \frac{\sin^{n-2} \theta}{(\bar{\rho}^2 + 1 - 2\bar{\rho} \cos \theta)^{n/2}} d\theta.$$

According to [8, (A.25)], we have

$$(2.19) \quad \lambda(\bar{\rho}) = \frac{1}{\bar{\rho}^{n-2}(\bar{\rho}^2 - 1)} \int_0^\pi \sin^{n-2} \sigma d\sigma.$$

Then, we derive from (2.18) and (2.19) that

$$(2.20) \quad \int_{r < |\mathbf{z}| < \gamma} P_r(\mathbf{x}, \mathbf{z}) d\mathbf{z} = 2\pi \tilde{C}_n^\alpha (\bar{r}^2 - 1)^{\alpha/2} \prod_{k=1}^{n-2} \int_0^\pi \sin^k \theta d\theta \int_r^\gamma \frac{\bar{\rho}}{(\bar{\rho}^2 - \bar{r}^2)^{\alpha/2} (\bar{\rho}^2 - 1)} d\bar{\rho}.$$

Recall the formulas [8, Proposition A.10],

$$(2.21) \quad \pi \prod_{k=1}^{n-2} \int_0^\pi \sin^k \theta d\theta = \frac{\pi^{n/2}}{\Gamma(n/2)}.$$

In view of (2.20) and (2.21), we make the change of variable $t = (\bar{\rho}/\bar{r})^2 - 1$, and obtain

$$(2.22) \quad \int_{r < |\mathbf{z}| < \gamma} P_r(\mathbf{x}, \mathbf{z}) d\mathbf{z} = \frac{\pi^{n/2}}{\Gamma(n/2)} \tilde{C}_n^\alpha \int_0^{\frac{\gamma^2}{r^2} - 1} \frac{1}{(1+t)t^{\alpha/2}} dt,$$

let $\tilde{t} = 1/(1+t)$, then we have

$$(2.23) \quad \int_{r < |\mathbf{z}| < \gamma} P_r(\mathbf{x}, \mathbf{z}) d\mathbf{z} = \frac{\pi^{n/2}}{\Gamma(n/2)} \tilde{C}_n^\alpha \int_{\frac{r^2}{\gamma^2}}^1 \tilde{t}^{-\alpha/2} (1-\tilde{t})^{\alpha/2-1} d\tilde{t}.$$

Thanks to P_r is a probability density function (cf. (2.9)), then

$$(2.24) \quad \int_{r < |\mathbf{z}| < \gamma} P_r(\mathbf{x}, \mathbf{z}) d\mathbf{z} = \frac{\pi^{n/2}}{\Gamma(n/2)} \tilde{C}_n^\alpha \left[B\left(1 - \frac{\alpha}{2}, \frac{\alpha}{2}\right) - B\left(\frac{r^2}{\gamma^2}; 1 - \frac{\alpha}{2}, \frac{\alpha}{2}\right) \right] := \omega \in (0, 1).$$

Moreover, by the inverse of the distribution function and (2.5), we can easily obtain the desired result (2.17). \square

We reformulate Green's function into a concise form, which helps us evaluate the weight function $\zeta(\mathbf{x})$ of each ball more easily. In the following Lemma, we use $r = r_i$ for simplicity.

LEMMA 2.7. *For $r > 0$, $\zeta(\mathbf{x})$ in Lemma 2.3 can be computed by*

$$(2.25) \quad \zeta(\mathbf{x}) = \widehat{C}_n^\alpha \int_{\mathbb{B}_r^n} |\mathbf{y} - \mathbf{x}|^{\alpha-n} \left[B\left(\frac{n-\alpha}{2}, \frac{\alpha}{2}\right) - B\left(\varrho^*(\mathbf{x}, \mathbf{y}); \frac{n-\alpha}{2}, \frac{\alpha}{2}\right) \right] d\mathbf{y}.$$

In particular, if $\mathbf{x} = \mathbf{0}$, we have

$$(2.26) \quad \zeta(\mathbf{0}) = \frac{r^\alpha}{2^{\alpha-1} \Gamma^2(\frac{\alpha}{2})} \int_0^1 \bar{\rho}^{\alpha-1} \left[B\left(\frac{n-\alpha}{2}, \frac{\alpha}{2}\right) - B\left(\bar{\rho}^2; \frac{n-\alpha}{2}, \frac{\alpha}{2}\right) \right] d\bar{\rho}.$$

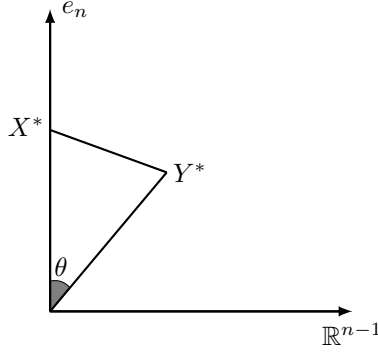


FIG. 3. The diagram of coordinate axes after rotation

Proof. In view of (2.3), we can rewritten the Green's function as

$$\begin{aligned}
Q_r(\mathbf{x}, \mathbf{y}) &= \widehat{C}_n^\alpha |\mathbf{y} - \mathbf{x}|^{\alpha-n} \int_0^{\varrho(\mathbf{x}, \mathbf{y})} \frac{t^{\alpha/2-1}}{(1+t)^{\frac{\alpha}{2}}} dt \\
&= \widehat{C}_n^\alpha |\mathbf{y} - \mathbf{x}|^{\alpha-n} \int_{\varrho^*(\mathbf{x}, \mathbf{y})}^1 \left(\frac{1}{m} - 1\right)^{\alpha/2-1} \left(\frac{1}{m}\right)^{-\frac{\alpha}{2}} \frac{1}{m^2} dm \\
&= \widehat{C}_n^\alpha |\mathbf{y} - \mathbf{x}|^{\alpha-n} \int_{\varrho^*(\mathbf{x}, \mathbf{y})}^1 m^{\frac{n-\alpha}{2}-1} (1-m)^{\alpha/2-1} dm \\
&= \widehat{C}_n^\alpha |\mathbf{y} - \mathbf{x}|^{\alpha-n} \left[B\left(\frac{n-\alpha}{2}, \frac{\alpha}{2}\right) - B\left(\varrho^*(\mathbf{x}, \mathbf{y}); \frac{n-\alpha}{2}, \frac{\alpha}{2}\right) \right],
\end{aligned}$$

where

$$\varrho^*(\mathbf{x}, \mathbf{y}) = \frac{r^2 |\mathbf{x} - \mathbf{y}|^2}{(r^2 - |\mathbf{x}|^2)(r^2 - |\mathbf{y}|^2) + r^2 |\mathbf{x} - \mathbf{y}|^2}.$$

This together with (2.7) yields

$$\zeta(\mathbf{x}) = \widehat{C}_n^\alpha \int_{\mathbb{B}_r^n} |\mathbf{y} - \mathbf{x}|^{\alpha-n} \left[B\left(\frac{n-\alpha}{2}, \frac{\alpha}{2}\right) - B\left(\varrho^*(\mathbf{x}, \mathbf{y}); \frac{n-\alpha}{2}, \frac{\alpha}{2}\right) \right] d\mathbf{y}.$$

Moreover, we obtain from (2.8) that

$$(2.27) \quad \widetilde{Q}_r(\mathbf{x}, \mathbf{y}) = \frac{\widehat{C}_n^\alpha |\mathbf{y} - \mathbf{x}|^{\alpha-n} \left[B\left(\frac{n-\alpha}{2}, \frac{\alpha}{2}\right) - B\left(\varrho^*(\mathbf{x}, \mathbf{y}); \frac{n-\alpha}{2}, \frac{\alpha}{2}\right) \right]}{\zeta(\mathbf{x})}.$$

In particular, if $\mathbf{x} = \mathbf{0}$, we have

$$\begin{aligned}
\zeta(\mathbf{0}) &= \widehat{C}_n^\alpha \int_{\mathbb{B}_r^n} |\mathbf{y}|^{\alpha-n} \left[B\left(\frac{n-\alpha}{2}, \frac{\alpha}{2}\right) - B(|\mathbf{y}|^2; \frac{n-\alpha}{2}, \frac{\alpha}{2}) \right] d\mathbf{y} \\
&= 2\pi \widehat{C}_n^\alpha \prod_{k=1}^{n-2} \int_0^\pi \sin^k \theta d\theta \int_0^r \rho^{\alpha-1} \left[B\left(\frac{n-\alpha}{2}, \frac{\alpha}{2}\right) - B(\rho^2; \frac{n-\alpha}{2}, \frac{\alpha}{2}) \right] d\rho \\
&= \frac{1}{2^{\alpha-1} \Gamma^2\left(\frac{\alpha}{2}\right)} \int_0^r \rho^{\alpha-1} \left[B\left(\frac{n-\alpha}{2}, \frac{\alpha}{2}\right) - B(\rho^2; \frac{n-\alpha}{2}, \frac{\alpha}{2}) \right] d\rho,
\end{aligned}$$

We then conclude that the desired result (2.26) holds under substitution $\rho = r\tilde{\rho}$. This ends the proof. \square

Remark 2.8. It should be pointed out that $\zeta(\mathbf{0})$ can be accurately computed by Jacobi-Gauss quadrature over the interval $(0, 1)$ with index $(0, \alpha - 1)$. For convenience, in actual computations we adopt the Monte Carlo integration for the calculation of the integral $\zeta(\mathbf{x})$.

2.3.2. The Monte Carlo method. In our simulation, the explicit expression of density functions $P_r(\mathbf{x}, \mathbf{z})$ and $\tilde{Q}(\mathbf{x}, \mathbf{y})$ play an essential role in constructing transition probabilities for a sequence of discrete points outside the ball and the random variables inside the ball, respectively. We now describe the implementations of the Monte Carlo method for the solution of (1.3). For any given point $\mathbf{x}_0 \in \Omega$, to evaluate $u(\mathbf{x}_0)$, we first calculate the shortest distance $r_1 = \text{dist}(\mathbf{x}_0, \Gamma_\varepsilon)$ from \mathbf{x}_0 to the domain Γ_ε , and then draw a inside ball $\mathbb{B}_{r_1}^n$ tangent to the domain Γ_ε centered at \mathbf{x}_0 with radius r_1 . Next, we construct a random variable X_1 (located at \mathbf{x}_1) for outside sphere $\mathbb{B}_{r_1}^n$ associated with the corresponding density function $P_{r_1}(\mathbf{x}_0, \mathbf{x}_1)$, and construct another random variable Y_1 (located at \mathbf{y}_1) for inside the ball $\mathbb{B}_{r_1}^n$ associated with the density function $\tilde{Q}(\mathbf{x}_0, \mathbf{y}_1)$.

- If $X_1 = \mathbf{x}_1$ is outside the region Ω , then the value of $u(\mathbf{x}_0)$ can be expressed as:

$$u(\mathbf{x}_0) = \zeta(\mathbf{x}_0)\mathbb{E}_{\mathbf{x}_0}[f(Y_1)] + \mathbb{E}_{\mathbf{x}_0}[g(X_1)].$$

If $X_1 = \mathbf{x}_1$ is inside the region Ω , we compute the distance $r_2 = \text{dist}(\mathbf{x}_1, \Gamma_\varepsilon)$ from \mathbf{x}_1 to the domain Γ_ε , and draw a new inside ball $\mathbb{B}_{r_2}^n$ tangent to the boundary Γ_ε centered at \mathbf{x}_1 with the radius r_2 . Next, construct a random variable X_2 for the outside ball $\mathbb{B}_{r_2}^n$ associated with the density function is $P_{r_2}(\mathbf{x}_1, \mathbf{x}_2)$, and construct another random variable Y_2 for the inside the ball $\mathbb{B}_{r_2}^n$ associated with the density function $\tilde{Q}(\mathbf{x}_1, \mathbf{y}_2)$.

- If $X_2 = \mathbf{x}_2$ is outside the region Ω , then the value of $u(\mathbf{x}_0)$ can be expressed as:

$$u(\mathbf{x}_0) = \zeta(\mathbf{x}_0)\mathbb{E}_{\mathbf{x}_0}[f(Y_1)] + \zeta(\mathbf{x}_1)\mathbb{E}_{\mathbf{x}_1}[f(Y_1)|X_1] + \mathbb{E}_{\mathbf{x}_0}[g(X_2)].$$

To this ends, we let

$$(2.28) \quad u(X_k) = \zeta(X_k)\mathbb{E}_{\mathbf{x}}[f(Y_{k+1})|X_k] + \mathbb{E}_{\mathbf{x}}[u(X_{k+1})|X_k],$$

where we used the conditional expectations in the above as the densities are determined by the position of X_k .

- By an induction argument, we suppose that the process exists in the region Ω on m^* -th step, then the solution of (1.3) is given by

$$(2.29) \quad \begin{aligned} u(\mathbf{x}_0) &= \mathbb{E}_{\mathbf{x}}[u(X_0)] = \mathbb{E}_{\mathbf{x}}[u(X_{m^*})] + \sum_{k=0}^{m^*-1} \mathbb{E}_{\mathbf{x}}[u(X_k) - u(X_{k+1})] \\ &= \mathbb{E}_{\mathbf{x}}[u(X_{m^*})] + \sum_{k=0}^{m^*-1} \mathbb{E}_{\mathbf{x}}[u(X_k) - \mathbb{E}_{\mathbf{x}}[u(X_{k+1})|X_k]], \end{aligned}$$

where we used the fact that $\mathbb{E}_{\mathbf{x}}[u(X_{k+1})|X_k] = \mathbb{E}_{\mathbf{x}}[u(X_{k+1})]$ in the last equality above.

By (2.28), we can rewrite the solution as follows:

$$(2.30) \quad u(\mathbf{x}_0) = \mathbb{E}_{\mathbf{x}}[u(X_{m^*})] + \sum_{k=0}^{m^*-1} \zeta(X_k)\mathbb{E}_{\mathbf{x}}[f(Y_{k+1})].$$

Then, we can construct a Monte Carlo procedure based on the random sample as

$$(2.31) \quad S_i = g(X_{m^*}^i) + \sum_{k=0}^{m^*-1} \zeta(X_k^i)f(Y_{k+1}^i).$$

where the index i represents the i -th experiment. By (2.30) and (2.31), we have $u(\mathbf{x}_0) \approx E(S_i)$.

COROLLARY 2.9. *Let $r > 0$ and $\alpha \in (0, 2]$, and assume that $f \in L^1_\alpha(\Omega) \cap C(\overline{\Omega})$ and $g \in L^1_\alpha(\mathbb{R}^n \setminus \Omega)$, then the solution of (1.3) in $L^1_\alpha(\mathbb{R}^n)$ can be computed by*

$$u(\mathbf{x}) = \lim_{N \rightarrow \infty} \frac{1}{N} \sum_{i=1}^N S_i = \mathbb{E}_{\mathbf{x}} \left[g(X_{m^*}^i) + \sum_{k=0}^{m^*-1} \zeta(X_k^i) f(Y_{k+1}^i) \right], \quad \mathbf{x} \in \Omega.$$

Finally, the above derivations lead to the Monte Carlo algorithm outlined in **Algorithm 2.1**.

Algorithm 2.1 Monte Carlo method for (1.3).

Input: (1). the number of paths N ;
(2). the threshold of the boundary ε ;
(3). the index α and the initial point $\mathbf{x}_0 \in \Omega$;
for i in $1 : N$ **do**
Set $k = 0$;
Step 1. Calculate the $r_1 = d(\mathbf{x}_k, \partial\Omega)$;
Step 2. Construct the random variable X_{k+1}^i with a density function $P_{r_{k+1}}(\mathbf{x}_k, \mathbf{x}_{k+1}^i)$ by (2.2);
Step 3. Construct the random variable Y_{k+1}^i with a density function $\tilde{Q}_r(\mathbf{x}_k^i, \mathbf{y}_{k+1}^i)$ by (2.27);
Step 4. Calculate the $r_{k+2} = d(\mathbf{x}_{k+1}^i, \partial\Omega)$.
if $r_{k+2} \leq 0$ **then**
 $m^* = k + 1$, compute S_i by (2.31).
else
 $k = k + 1$, return to Step 4;
end if
end for
Output: $u(\mathbf{x}_0) \approx \frac{1}{N} \sum_{i=1}^N S_i$.

3. The error estimate and theoretical analysis of the algorithm. The error estimates for the proposed method on the irregular domain appear to be very difficult. To fix the idea, we only focus on the error bound, in expectation form, of the proposed algorithm for the approximation of fractional Poisson equations (1.3) on the ball in arbitrary dimensions. Moreover, we will also analyze the effectiveness of the algorithm.

In this section, by (2.14) and $\Omega = \mathbb{B}_r^n$, we have $\Gamma_\varepsilon = \bar{\mathbb{B}}_r^n \setminus \mathbb{B}_{r-\varepsilon}^n$. We first explore the relation between the width of layer Γ_ε and the error, which will be used for the error analysis later on.

LEMMA 3.1. *For any $\varepsilon > 0$, and let $u \in L^1_\alpha(\mathbb{R}^n)$, $f \in L^1_\alpha(\mathbb{B}_r^n) \cap C(\bar{\mathbb{B}}_r^n)$ and $g \in L^1_\alpha(\mathbb{R}^n \setminus \mathbb{B}_r^n)$ with $r > 0$ and $\alpha \in (0, 2]$, there holds*

$$(3.1) \quad |\mathbb{E}[g(X'_{m^*})] - \mathbb{E}[u(X_{m^*})]| \leq \frac{2^{1-\alpha} M}{\alpha \Gamma^2(\alpha/2)} \varepsilon^\alpha, \quad X_{m^*} \in \mathbb{R}^n \setminus \mathbb{B}_{r-\varepsilon}^n,$$

where

$$(3.2) \quad X'_{m^*} = \begin{cases} X_{m^*}, & \text{if } X_{m^*} \in \mathbb{R}^n \setminus \mathbb{B}_r^n, \\ \inf_{\chi \in \partial \mathbb{B}_r^n} \{|\chi - X_{m^*}|\}, & \text{if } X_{m^*} \in \mathbb{B}_r^n \setminus \mathbb{B}_{r-\varepsilon}^n. \end{cases}$$

Proof. Without loss of generality, we assume that $g(\mathbf{x}) = 0$, it is straightforward to extend this result to the non-homogeneous case, i.e., $g(\mathbf{x}) \neq 0$. For $X_{m^*} \in \mathbb{R}^n \setminus \mathbb{B}_r^n$, we can find that $u(X_{m^*}) = g(X'_{m^*})$, the conclusion is clearly valid. Next, we turn to prove the case $X_{m^*} \in \mathbb{B}_r^n$. By

using (2.19), (2.21), and (2.25), we can obtain that

$$\begin{aligned}
 \zeta(\mathbf{x}) &= \widehat{C}_n^\alpha \int_{\mathbb{B}_r^n} |\mathbf{y} - \mathbf{x}|^{\alpha-n} \left[B\left(\frac{n-\alpha}{2}, \frac{\alpha}{2}\right) - B\left(\varrho^*(\mathbf{x}, \mathbf{y}); \frac{n-\alpha}{2}, \frac{\alpha}{2}\right) \right] d\mathbf{y} \\
 &= \widehat{C}_n^\alpha \int_{\mathbb{B}_r^n} |\mathbf{y} - \mathbf{x}|^\alpha \cdot |\mathbf{y} - \mathbf{x}|^{-n} \left[B\left(\frac{n-\alpha}{2}, \frac{\alpha}{2}\right) - B\left(\varrho^*(\mathbf{x}, \mathbf{y}); \frac{n-\alpha}{2}, \frac{\alpha}{2}\right) \right] d\mathbf{y} \\
 &< \widehat{C}_n^\alpha \pi \prod_{k=1}^{n-3} \int_0^\pi \sin^k \theta d\theta \int_0^r \int_0^\pi (2r^2 - |\mathbf{x}|^2)^{\alpha/2} \frac{\rho^{n-1} \sin^{n-2} \theta}{(\rho^2 + |\mathbf{x}|^2 - 2|\mathbf{x}|\rho \cos \theta)^{n/2}} d\theta d\rho \\
 &= \widehat{C}_n^\alpha (2r^2 - 1)^{\alpha/2} \pi \prod_{k=1}^{n-3} \int_0^\pi \sin^k \theta d\theta \int_0^r \int_0^\pi \frac{\rho^{n-1} \sin^{n-2} \theta}{(\rho^2 + 1 - 2\rho \cos \theta)^{n/2}} d\theta d\rho \\
 (3.3) \quad &= \widehat{C}_n^\alpha (2r^2 - 1)^{\alpha/2} \pi \prod_{k=1}^{n-3} \int_0^\pi \sin^k \theta d\theta \int_0^r \frac{\rho^{n-1}}{\rho^{n-2}(\rho^2 - 1)} \int_0^\pi \sin^{n-2} \theta d\theta d\rho \\
 &= C_n^\alpha (2r^2 - 1)^{\alpha/2} \int_0^r \frac{\rho}{\rho^2 - 1} d\rho = C_n^\alpha / 2 (2r^2 - 1)^{\alpha/2} \int_0^r \frac{1}{\rho + 1} + \frac{1}{\rho - 1} d\rho \\
 &= C_n^\alpha / 2 (2r^2 - 1)^{\alpha/2} \ln |r^2 - 1|,
 \end{aligned}$$

where the constant $C_n^\alpha = 2^{2-\alpha} B(\frac{n-\alpha}{2}, \frac{\alpha}{2}) / \Gamma^2(\frac{\alpha}{2})$. By (2.6), (2.7), and (3.3), we find that for $\mathbf{y} \in \mathbb{B}_r^n \setminus \Gamma_\varepsilon$,

$$\begin{aligned}
 u(\mathbf{x}) &= \int_{\mathbb{B}_r^n \setminus \Gamma_\varepsilon} f(\mathbf{y}) Q_r(\mathbf{x}, \mathbf{y}) d\mathbf{y} \leq \int_{\mathbb{B}_r^n \setminus \Gamma_\varepsilon} |f(\mathbf{y})| Q_r(\mathbf{x}, \mathbf{y}) d\mathbf{y} \leq M \zeta(\mathbf{x}) \\
 &= C_n^\alpha M / 2 (2(r - \varepsilon)^2 - 1)^{\alpha/2} \ln |(r - \varepsilon)^2 - 1|.
 \end{aligned}$$

Retrospect to (2.30), if $X_{m^*} \in \Gamma_\varepsilon$, it is evident that

$$u(\mathbf{x}) = \zeta(X_{m^*}) \mathbb{E}_{\mathbf{x}}[f(Y_{m^*+1})] + \sum_{k=0}^{m^*-1} \zeta(X_k) \mathbb{E}_{\mathbf{x}}[f(Y_{k+1})],$$

which implies

$$\mathbb{E}_{\mathbf{x}}[u(X_{m^*})] = u(\mathbf{x}) - \sum_{k=0}^{m^*-1} \zeta(X_k) \mathbb{E}_{\mathbf{x}}[f(Y_{k+1})] \leq \int_{\mathbb{B}_{r_{m^*}}^n} f(\mathbf{y}) Q_r(\mathbf{x}, \mathbf{y}) d\mathbf{y} \leq M \int_{\mathbb{B}_{r_{m^*}}^n} Q_r(\mathbf{x}, \mathbf{y}) d\mathbf{y}.$$

Moreover, by (2.7) and (2.26), we find that

$$\begin{aligned}
 \mathbb{E}[u(X_{m^*})] &\leq \frac{M}{2^{\alpha-1} \Gamma^2(\frac{\alpha}{2})} \int_0^\varepsilon \rho^{\alpha-1} \left[B\left(\frac{n-\alpha}{2}, \frac{\alpha}{2}\right) - B\left(\rho^2; \frac{n-\alpha}{2}, \frac{\alpha}{2}\right) \right] d\rho \\
 (3.4) \quad &\leq \frac{M}{2^{\alpha-1} \Gamma^2(\frac{\alpha}{2})} \int_0^\varepsilon \rho^{\alpha-1} d\rho = \frac{2^{1-\alpha} M}{\alpha \Gamma^2(\alpha/2)} \varepsilon^\alpha.
 \end{aligned}$$

Then, for $X_{m^*} \in \Gamma_\varepsilon$,

$$|\mathbb{E}[u(X_{m^*})] - \mathbb{E}[g(X'_{m^*})]| \leq \frac{2^{1-\alpha} M}{\alpha \Gamma^2(\alpha/2)} \varepsilon^\alpha.$$

A combination of the above estimates leads to desired result. \square

LEMMA 3.2. For any $\varepsilon > 0$, and assume that $u \in L_\alpha^1(\mathbb{R}^n)$, $f \in L_\alpha^1(\mathbb{B}_r^n) \cap C(\overline{\mathbb{B}_r^n})$ and $g \in L_\alpha^1(\mathbb{R}^n \setminus \mathbb{B}_r^n)$ with $r > 0$ and $\alpha \in (0, 2]$, then we have

$$(3.5) \quad \mathbb{E}_{\mathbf{x}}[\bar{S} - u(\mathbf{x})]^2 \leq \mathcal{O}(N^{-1} + \varepsilon^{2\alpha}).$$

Proof. It is known that the random sample S_i is independently and identically distributed, so $(S_i, S_j) = 0$ for $i \neq j$. Then, we have

$$\text{Var}(\bar{S}) = \text{Var}\left(\frac{1}{N} \sum_{i=1}^N S_i\right) = \frac{1}{N^2} \sum_{i=1}^N \text{Var}(S_i) = \mathcal{O}(N^{-1}).$$

Thanks to Lemma 3.1, we arrive at

$$\begin{aligned} \mathbb{E}_{\mathbf{x}}[\bar{S} - u(\mathbf{x})]^2 &= \mathbb{E}_{\mathbf{x}}\{\bar{S} - \mathbb{E}[\bar{S}] + \mathbb{E}[\bar{S}] - u(\mathbf{x})\}^2 \\ &\leq 2\mathbb{E}_{\mathbf{x}}\{\bar{S} - \mathbb{E}[\bar{S}]\}^2 + 2\mathbb{E}_{\mathbf{x}}\{\mathbb{E}[\bar{S}] - u(\mathbf{x})\}^2 \\ &\leq 2\text{Var}(\bar{S}) + 2\left\{\frac{1}{N} \sum_{i=1}^N \mathbb{E}[g(X_{m^*}^i) + \sum_{k=0}^{n^*-1} \zeta(X_k^i) f(Y_{k+1}^i)] \right. \\ &\quad \left. - \frac{1}{N} \sum_{i=1}^N \left(\mathbb{E}[u(X_{m^*}^i)] - \sum_{k=0}^{n^*-1} \zeta(X_k^i) \mathbb{E}[f(Y_{k+1}^i)]\right)\right\}^2 \\ (3.6) \quad &\leq 2\text{Var}(\bar{S}) + \frac{2}{N^2} \left\{ \sum_{i=1}^N \left| \mathbb{E}[g(X_{m^*}^i)] - \mathbb{E}[u(X_{m^*}^i)] \right| \right\}^2. \end{aligned}$$

Therefore, we can bound the error from the above estimates. \square

LEMMA 3.3. *For any $\varepsilon > 0$, $\alpha \in (0, 2]$, and given initial point $\mathbf{x} \in \mathbb{B}_r^n$ with $r > 0$, then the probability of the point \mathbf{x} leaving the domain \mathbb{B}_r^n is positive, that is,*

$$(3.7) \quad \mathbb{E}_{\mathbf{x}}(m^*) < 1 + \frac{q_*}{(1 - p_*)^2},$$

where the constants

$$\begin{aligned} p_* &:= p_*(n, \alpha, r, \varepsilon) = \frac{\pi^{n/2}}{\Gamma(n/2)} \tilde{C}_n^\alpha \left[B\left(\frac{\alpha}{2}, 1 - \frac{\alpha}{2}\right) - B\left(\frac{\varepsilon^2}{r^2}; \frac{\alpha}{2}, 1 - \frac{\alpha}{2}\right) \right], \\ q_* &:= q_*(n, \alpha, r, \varepsilon) = 1 - \frac{\pi^{n/2}}{\Gamma(n/2)} \tilde{C}_n^\alpha \left[B\left(\frac{\alpha}{2}, 1 - \frac{\alpha}{2}\right) - B\left(\frac{(r - \varepsilon)^2}{r^2}; \frac{\alpha}{2}, 1 - \frac{\alpha}{2}\right) \right]. \end{aligned}$$

with \tilde{C}_n^α given in (2.5).

Proof. Denote by $\mathbb{B}_{d_i}^{n, \mathbf{x}_i}$ the i -th inside ball centered at \mathbf{x}_i and tangent the domain Γ_ε , that is, the ball $\mathbb{B}_{d_i}^{n, \mathbf{x}_i}$ tangent the boundary $\partial\mathbb{B}_{r-\varepsilon}^n$. Then, it is easy to check that the radius of the i -th ball is $d_i = r - |\mathbf{x}_i| - \varepsilon$. We set $p(d_i, \mathbf{x}_i, \mathbf{y}_i) = \Pr\{\mathbf{y}_i \in \mathbb{B}_{r-\varepsilon}^n \setminus \mathbb{B}_{d_i}^{n, \mathbf{x}_i} | \mathbf{x}_i \in \mathbb{B}_{d_i}^{n, \mathbf{x}_i}\}$, which represents the probability that the $(i+1)$ -th ball remains inside the region $\mathbb{B}_{r-\varepsilon}^n$ under the condition that the i -th ball is inside the region $\mathbb{B}_{r-\varepsilon}^n$. By (2.24), we have

$$p(d_i, \mathbf{x}_i, \mathbf{y}_i) = \int_{d_i < |\mathbf{y}_i| < r - \varepsilon} P_{d_i}(\mathbf{x}_i, \mathbf{y}_i) d\mathbf{y}_i = \frac{\pi^{n/2}}{\Gamma(n/2)} \tilde{C}_n^\alpha \left[B\left(\frac{\alpha}{2}, 1 - \frac{\alpha}{2}\right) - B\left(\frac{d_i^2}{(r - \varepsilon)^2}; \frac{\alpha}{2}, 1 - \frac{\alpha}{2}\right) \right].$$

To simplify the notations, we use $p_i = p(d_i, \mathbf{x}_i, \mathbf{y}_i) \in (0, 1)$, and $q_i = 1 - p_i$, then

$$\begin{aligned} \mathbb{E}_{\mathbf{x}}(m^*) &= \sum_{k=1}^M k \mathbb{P}_{\mathbf{x}}(m^* = k) = q_1 + 2p_1q_2 + 3p_1p_2q_3 + \cdots + Mp_1p_2 \cdots p_{M-1}q_M = \sum_{k=1}^M k \prod_{i=1}^{k-1} p_i q_k \\ &= \sum_{k=1}^M k \prod_{i=1}^{k-1} \frac{\pi^{n/2}}{\Gamma(n/2)} \tilde{C}_n^\alpha \left[B\left(\frac{\alpha}{2}, 1 - \frac{\alpha}{2}\right) - B\left(\frac{d_i^2}{(r - \varepsilon)^2}; \frac{\alpha}{2}, 1 - \frac{\alpha}{2}\right) \right] \\ &\quad \cdot \left\{ 1 - \frac{\pi^{n/2}}{\Gamma(n/2)} \tilde{C}_n^\alpha \left[B\left(\frac{\alpha}{2}, 1 - \frac{\alpha}{2}\right) - B\left(\frac{d_k^2}{(r - \varepsilon)^2}; \frac{\alpha}{2}, 1 - \frac{\alpha}{2}\right) \right] \right\}. \end{aligned}$$

Let $p_* = \max_i \{p_i\}$ and $q_* = \max_j \{q_j\}$, it is easy to verify that

$$\begin{aligned}
 \mathbb{E}_x(m^*) &< q_1 + 2p_1q_* + 3p_1p_*q_* + 4p_1p_*^2q_* + \cdots + Mp_1p_*^{M-1}q_* \\
 &= 1 - 2p_1 + p_1(1 + 2q_* + 3p_*q_* + 4p_*^2q_* + \cdots + Mp_*^{M-1}q_*) \\
 (3.8) \quad &= 1 - 2p_1 + p_1\left(1 + \frac{q_*}{p_*}(1 + 2p_* + 3p_*^2 + 4p_*^3 + \cdots + Mp_*^{M-1}) - \frac{q_*}{p_*}\right) \\
 &= 1 - 2p_1 + p_1\left(1 + \frac{q_*}{p_*}\partial_{p_*}(p_* + p_*^2 + p_*^3 + p_*^4 + \cdots + p_*^M) - \frac{q_*}{p_*}\right) \\
 &= 1 - 2p_1 + p_1\left(1 + \frac{q_*}{p_*}\partial_{p_*}\left(\frac{p_*(1-p_*^M)}{1-p_*}\right) - \frac{q_*}{p_*}\right).
 \end{aligned}$$

As $0 < p_*, q_* < 1$, it is evident that $p_*^M \rightarrow 0$ for $M \rightarrow \infty$, which implies $\frac{p_*(1-p_*^M)}{1-p_*} \rightarrow \frac{p_*}{1-p_*}$. A direct computation gives $\partial_{p_*}\left(\frac{p_*}{1-p_*}\right) = \frac{1}{(1-p_*)^2}$, then we find from (3.8) that

$$\mathbb{E}_x(m^*) < 1 - p_1 + \frac{p_1 q_*}{p_*(1-p_*)^2} < 1 + \frac{p_1 q_*}{p_*(1-p_*)^2} < 1 + \frac{q_*}{(1-p_*)^2},$$

where we used the fact that $p_1 < p_*$ in the last inequality. This ends the proof. \square

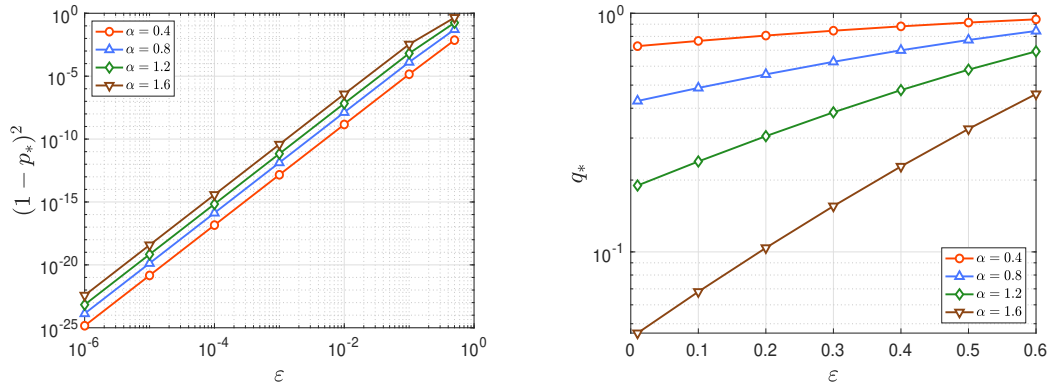


FIG. 4. Left: the value $1 - p_*^2$ versus ε ; Right: the value q_* versus ε .

In Fig. 4, we plot the magnitude of $(1-p_*)^2$ and q_* against various ε in the log-log and semi-log scale, respectively. We observe that the values of $(1-p_*)^2$ and q_* increase as ε increase. They indicate that the greater the width ε , the lower the probability that the ball in the domain Ω will remain in the next step. On the contrary, the thicker the width ε , the higher probability the small ball will leave the domain Ω in the next step. We observe that they are consistent with the theoretical result.

4. Numerical Results. We present ample numerical results to illustrate our numerical methods, in particular, the Algorithm 2.1 for computing solutions of fractional Poisson equation (1.3). These examples include smooth functions and functions with low regularities at the boundary, and we also checked the efficiency of the proposed method in two dimensions and even in 10-dimensions. Note that all computations below were performed in MATLAB R2018a on a 64-bit Macbook Pro laptop with a quad-core Intel Core i5 processor at 2.3 GHz and 8GB of RAM. For the sake of simplicity, we work on the problem with exact solutions. In what follows, all the numerical results are obtained by Algorithm 2.1, and all the numerical errors are computed via randomly selected

points $\{\mathbf{x}_i\}_{i=1}^N$ with $N = 10000$ as below

$$\text{Error} = \frac{1}{N} \left(\sum_{i=1}^N (u(\mathbf{x}_i) - u_*(\mathbf{x}_i))^2 \right)^{\frac{1}{2}},$$

where $u_*(\mathbf{x})$ denote the numerical solution. The other parameter are set to be $\varepsilon = 10^{-6}$.

Example 1. (Exact solution in 2D with homogeneous BCs) We first consider (1.3) on a unit disk $\Omega = \mathbb{B}_1^2$ with the following exact solutions:

$$(4.1) \quad u(\mathbf{x}) = (1 - |\mathbf{x}|^2)^{\frac{\alpha}{2}},$$

where $a_+ = \max\{a, 0\}$. According to [16], the source term reduce to a constant, i.e., $f = 2^\alpha \Gamma^2(\frac{\alpha}{2} + 1)$. In this case, the nonlocal boundary condition becomes homogeneous, that is, $g(\mathbf{x}) = 0$ in Ω^c .

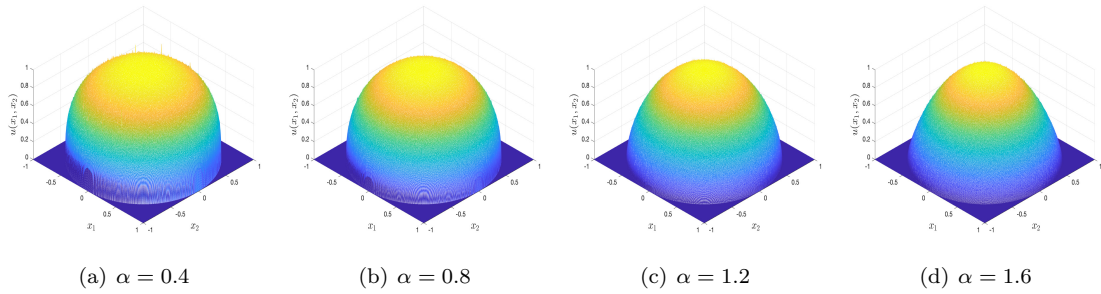


FIG. 5. Profiles of the numerical solutions with various α .

In order to demonstrate the efficiency of the proposed algorithm, we plot in Fig. 5 the profiles of numerical solutions with $\alpha = 0.4, 0.8, 1.2, 1.6$, in which we compute the approximate result at each given point $\mathbf{x} = (x_1, x_2)$ by employing 5000 paths. The exact solution has singularity near the boundary and behaves like $\text{dist}(\mathbf{x}, \partial\Omega)^{\frac{\alpha}{2}}$, where $\text{dist}(\mathbf{x}, \partial\Omega)$ denotes the distance function from \mathbf{x} to the boundary $\partial\Omega$. It can be seen from Fig. 5, with the decrease of the index α , the singular layers near the boundary are thinner and sharper as expected. We note that the computational complexity of the algorithm is $\mathcal{O}(N)$, where N represents the number of paths we set.

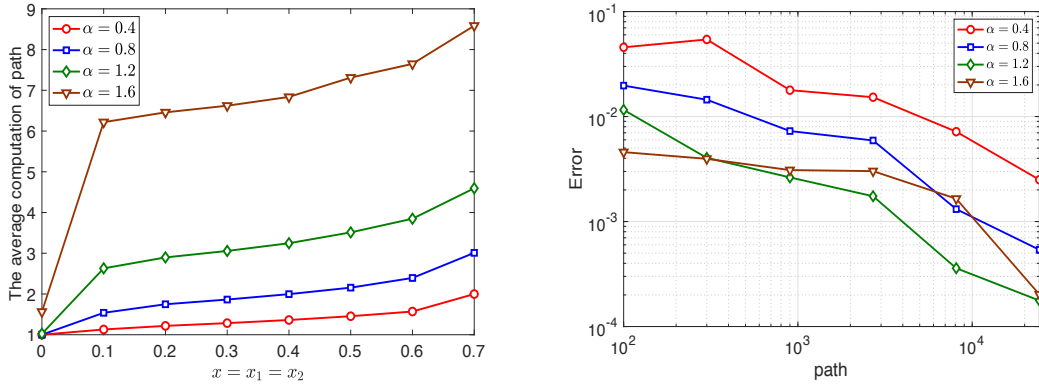


FIG. 6. Simulation for two-dimension. Left: the average number of steps for fixed point with various α ; Right: numerical errors against ε .

In Fig. 6 (left), we shows the average number of iterations required for each path when calculating $u(\mathbf{x})$ with different α , that is, the average of steps required for point \mathbf{x} to escape from domain \mathbb{B}_1^2 . We observe that when the starting point is farther away from the center, it will need more iterations, as the corresponding circle is smaller for the point near the boundary. In other words, the larger the area of $\mathbb{B}_1^2 \setminus \mathbb{B}_{r_1}^2$ will be, and the more likely the next point will fall in this area. In addition, when all conditions are set to be the same, as expected, the number of iterations increases as α increases. As α tends to 2, the distance from a fixed point \mathbf{x} to the next point will be smaller, which leads to an increase in the number of iterations escaping from region \mathbb{B}_1^2 . In Fig. 6 (right), we plot the numerical errors, in log-log scale, against the number of paths with different fractional order α .

Example 2. (Source problem in 2D with non-homogeneous BCs) We next consider (1.3) with the following source functions:

$$(4.2) \quad f(\mathbf{x}) = \Gamma(2 + \alpha)_2 F_1 \left(\frac{2 + \alpha}{2}, \frac{3 + \alpha}{2}; 1; -|\mathbf{x}|^2 \right), \quad \text{on } \Omega = \mathbb{B}_1^2.$$

Fortunately, we have the explicit expression of exact solution $u(\mathbf{x}) = (1 + |\mathbf{x}|^2)^{-\frac{3}{2}}$ on \mathbb{R}^2 , which implies the nonhomogeneous boundary condition $g(\mathbf{x}) = u(\mathbf{x})$ on Ω^c .

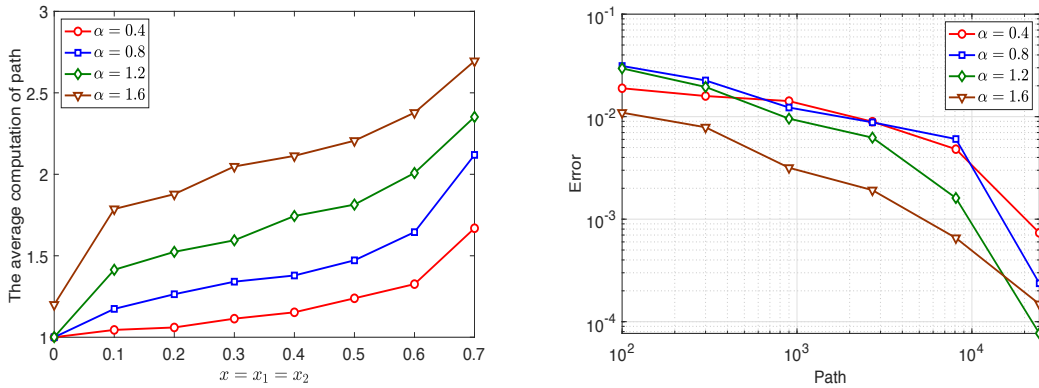


FIG. 7. Simulation for two-dimension. Left: the average number of steps for fixed point with various α ; Right: numerical errors against the number of path with various α .

We use the Monte Carlo method suggested in Algorithm 2.1 to resolve this problem. In Fig. 7 (left), we plot the average number of iterations required for each path to simulate $u(\mathbf{x})$ with various fractional order α . The errors of numerical solution against the number of path with various α in log-log scale are shown in Fig. 7 (right). We observe that the numerical errors decay as the number of path increases. They indicate that our algorithm is very effective for IFL with nonhomogeneous BCs.

Example 3. (Exact solution in 10D with homogeneous BCs) Again, we consider (1.3) in high dimensions with the following exact solutions (cf. [16]):

$$(4.3) \quad u(\mathbf{x}) = (1 - |\mathbf{x}|)_+^{\frac{\alpha}{2}}, \quad \mathbf{x} \in \Omega = \mathbb{B}_1^{10},$$

then the source term reduce to a constant, i.e., $f(\mathbf{x}) = 2^\alpha \Gamma(1 + \frac{\alpha}{2}) \Gamma(\frac{n+\alpha}{2}) / \Gamma(\frac{n}{2})$. In this case, the nonlocal boundary condition is homogeneous, that is, $g(\mathbf{x}) = 0$ in Ω^c .

In Fig. 8 (left), we plot the average number of iterations required for each path when calculating $u(\mathbf{x})$ for different α . The numerical errors of numerical solution against the number of path with

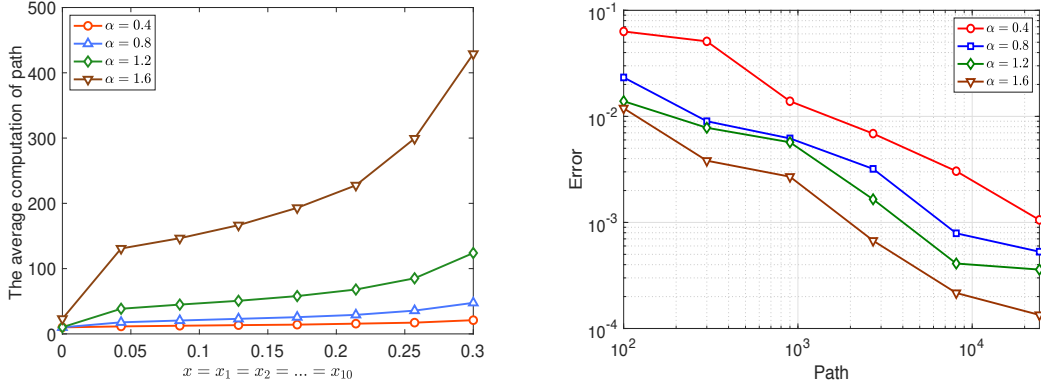


FIG. 8. Simulation for 10-dimension. Left: the average number of steps for fixed point with various α ; Right: numerical errors against the number of path with various α .

various α in log-log scale are plotted in Fig. 8 (right). As with the results in 2D, Fig. 8 demonstrate that the average number of iterations required to compute $u(\mathbf{x})$ for the same α increases as $|\mathbf{x}|$ increases for 10-dimensional problems. For a given point $\mathbf{x} \in \Omega$, the average number of iterations required increases in proportion to the value of fractional order α . Moreover, the relationship between the number of paths and numerical error is consistent with the two-dimensional problem. In particular, they indicate that our algorithm is very effective and stable for high dimensional problems. Indeed, this is one of the main advantages of the proposed method, which distinguish our approach from other existing methods for fractional PDEs.

Example 4. (IFL on irregular domains) In this example, we shall present the numerical results of our algorithm for IFL on irregular domains. To check the accuracy, we consider (1.3) with the following source function and boundary condition:

$$(4.4) \quad f(\mathbf{x}) = 2^\alpha \Gamma(1 + \alpha/2) {}_1F_1\left(\frac{2 + \alpha}{2}; 1; -|\mathbf{x}|^2\right), \quad \mathbf{x} \in \Omega; \quad g(\mathbf{x}) = e^{-|\mathbf{x}|^2}, \quad \mathbf{x} \in \Omega^c.$$

In this case, we take $\Omega = [-1, 1]^2 \setminus (0, 1]^2$, which represents an L-shaped domain. According to [34], we have the explicit expression of exact solution $u(\mathbf{x}) = e^{-|\mathbf{x}|^2}$ on Ω .

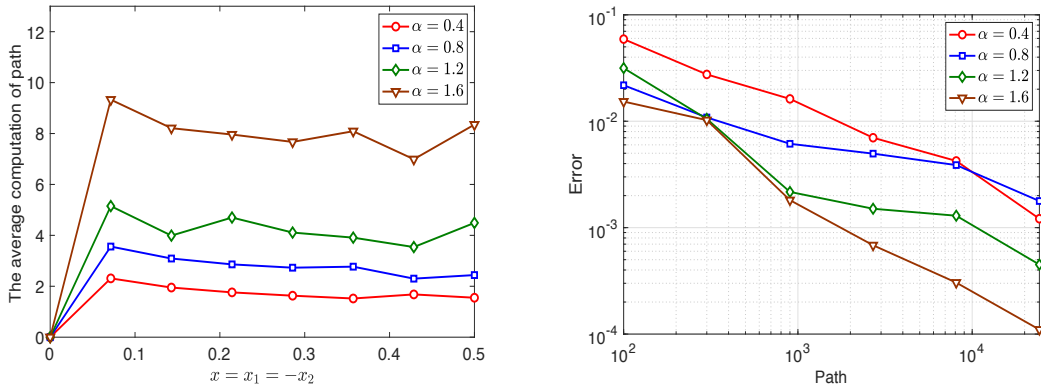


FIG. 9. Simulation for two-dimension on complex domains. Left: the average number of steps for fixed point with various α ; Right: numerical errors against the number of path with various α .

In Fig. 9 (left), we show the average number of iterations required for each path when calcu-

lating $u(\mathbf{x})$ for different fractional power α . We observe from Fig. 9 (left) that the average number of iterations for each path does not increase when $|\mathbf{x}| > 0.1$. For the L -shaped domain, with the increase of the coordinates of point \mathbf{x} along with the $(1, -1)$ -direction, the distance between the point and boundary first increases and then gradually decreases. Thus, the average number of iterations required for each path first increases and then gradually decreases. The numerical errors against the path number is listed in Fig. 9 (right). As expected, the numerical errors decay algebraically as the increase of the total path. These are consistent with our previous theoretical analysis results.

To show the efficiency of our method on the complex domains, we further consider the following three cases:

(i). For the stripe domain, we take

$$(4.5) \quad f(\mathbf{x}) = 2^\alpha \Gamma(1 + \frac{\alpha}{2}) (\cos^{\frac{\alpha}{3}}(c_2 \mathbf{x}) + \sin^{\frac{\alpha}{2}}(c_1 \mathbf{x})) \cos(-|\mathbf{x}|^2) \quad \text{on } \Omega,$$

where $c_1 = (\frac{\pi}{3}, -\frac{\pi}{4})$, $c_2 = (-\frac{\pi}{2}, \frac{2\pi}{3})$, $\mathbf{x} = (x_1, x_2)^T$, and Ω is the stripe domain on $[-5, 5] \times [-0.5, 0.5]$, the boundary condition can be set as $g(\mathbf{x}) = 0$ over Ω^c .

(ii). For regular hexagon domain, we take

$$(4.6) \quad f(\mathbf{x}) = \sin^2(c_1 \mathbf{x}) + \cos^2(c_2 \mathbf{x}) - (\alpha x_1 x_2)^3, \quad \text{on } \Omega,$$

where Ω is the regular hexagon domain on $[-1, 1]^2$, the boundary condition can be set as $g(\mathbf{x}) = 0$ over Ω^c .

(iii). For the annulus domain, we take

$$(4.7) \quad f(\mathbf{x}) = \cos(x_2^2 - 2x_1 x_2) - \sin(x_1^2 + 2x_1 x_2), \quad \text{on } \Omega,$$

where $\Omega = \{\mathbf{x} \in \mathbb{R}^2 : 0.3 < |\mathbf{x}|^2 < 1\}$ is the annulus domain, the boundary condition can be set as $g(\mathbf{x}) = 0$ over Ω^c .

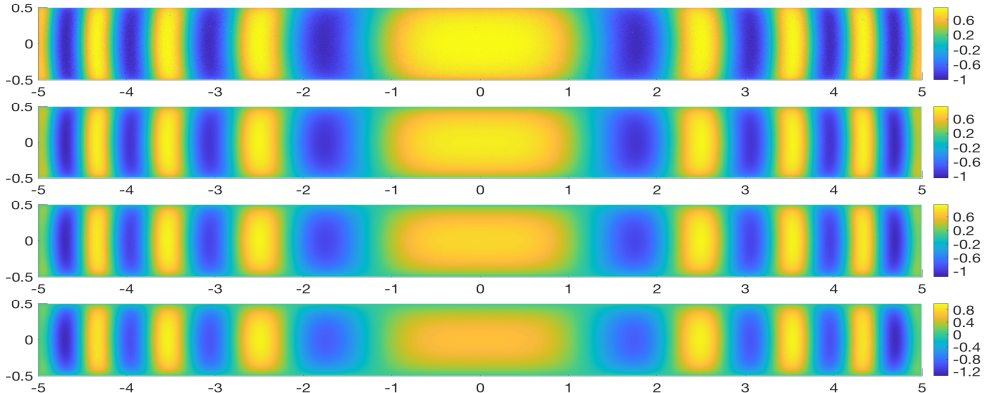


FIG. 10. Profiles of the numerical solutions zoomed in the stripe domain $[-5, 5] \times [-0.5, 0.5]$ with $\alpha = 0.4, 0.8, 1.2, 1.6$ (from top to bottom).

We use the proposed Monte Carlo method to calculate numerical solutions on three different shaped domains, and plot the corresponding profiles with various fractional order α in Fig. 10 and 11. We observe similar behaviors as in the circular domain case, and the singularity layer near the boundary becomes thinner as expected as the fractional power α decreases.

5. Conclusion. This paper proposes an efficient Monte Carlo method for solving fractional PDEs on bounded domains in arbitrary dimensions. The key to the efficiency of the Monte Carlo algorithm is to construct a new Feynman-Kac representation in expectation form based on the

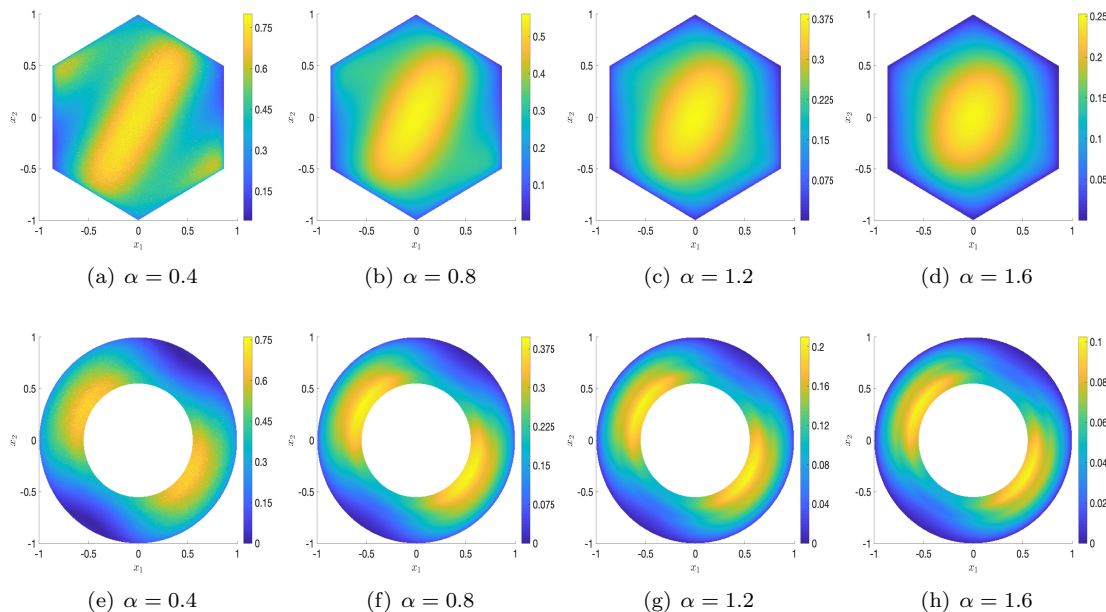


FIG. 11. Profiles of the numerical solutions with various α . Top: zoomed in the hexagon domain; Bottom: zoomed in the annulus domain.

explicit expressions of the Green functions. Then, we can avoid calculating the complex integrals associated with α -stable process function. The representation (2.12) allows us only to calculate the expectation of a random variable with known density functions, which enjoys the explicit expression of the Green functions. Each jump in the angular direction is distributed uniformly with the aid of the spherical coordinates, so we only need to appropriately add sample nodes in the angular direction with the increased dimensions. Consequently, the computation time will increase at a moderate pace with the increase of dimensions. Thus, this new process possesses fascinating merits for solving high-dimensional problems. More importantly, we prove the efficiency of our algorithm and establish the error analysis of the proposed method for the fractional Poisson equation. Our numerical experiments demonstrate that our algorithms are efficient and accurate. In addition, the Monte Carlo method allows us to use parallel computing to improve the calculation efficiency and significantly reduce the computation time.

The idea of the proposed Monte Carlo method can be extended to the time-dependent problems with Feynman-Kac representation in a similar setting. In the future, we can combine the proposed method with the deep neural network for solving the nonlocal models driven by a stochastic process.

Acknowledgments. C. Sheng would like to thank Professor Jie Shen at Purdue University for many valuable suggestions and enlightening discussions.

REFERENCES

- [1] G. ACOSTA AND J. P. BORTHAGARAY, *A fractional Laplace equation: regularity of solutions and finite element approximations*, SIAM J. Numer. Anal., 55 (2017), pp. 472–495.
- [2] M. AINSWORTH AND C. GLUSA, *Aspects of an adaptive finite element method for the fractional Laplacian: a priori and a posteriori error estimates, efficient implementation and multigrid solver*, Comput. Methods Appl. Mech. Engrg., 327 (2017), pp. 4–35.
- [3] JANICKI ALEKSANDER AND WERON ALEKSANDER, *Can one see α -stable variables and processes?*, Statist. Sci., 9 (1994), pp. 109–126.
- [4] A. BONITO, W. LEI, AND J. E. PASCIAK, *Numerical approximation of the integral fractional Laplacian*, Numer.

- Math., 142 (2019), pp. 235–278.
- [5] J. P. BORTHAGARAY, L. M. DEL PEZZO, AND S. MARTINEZ, *Finite element approximation for the fractional eigenvalue problem*, J. Sci. Comput., 77 (2018), pp. 308–329.
 - [6] J. P. BORTHAGARAY, D. LEYKEKHMEN, AND R. H. NOCHETTO, *Local energy estimates for the fractional Laplacian*, SIAM J. Numer. Anal., 59 (2021), pp. 1918–1947.
 - [7] D. BROCKMANN, L. HUFNAGEL, AND T. GEISEL, *The scaling laws of human travel*, Nature, 439 (2006), p. 462.
 - [8] C. BUCUR, *Some observations on the Green function for the ball in the fractional Laplace framework*, Commun. Pure Appl. Anal., 15 (2016), pp. 657–699.
 - [9] H. CHEN, Y. YU, J. JAWORSKI, N. TRASK, AND M. D’ELIA, *Data-driven learning of reynolds stress tensor using nonlocal models*, Bulletin of the American Physical Society, 66 (2021).
 - [10] L. CHEN, Z. MAO, AND H. LI, *Jacobi-Galerkin spectral method for eigenvalue problems of Riesz fractional differential equations*, arXiv preprint arXiv:1803.03556, (2018).
 - [11] K. L. CHUNG AND Z. X. ZHAO, *From Brownian motion to Schrödinger’s equation*, vol. 312 of Grundlehren der mathematischen Wissenschaften [Fundamental Principles of Mathematical Sciences], Springer-Verlag, Berlin, 1995.
 - [12] M. DAY, *Book Review: Functional integration and partial differential equations*, Bull. Amer. Math. Soc. (N.S.), 17 (1987), pp. 346–351.
 - [13] J. M. DELAURENTIS AND L. A. ROMERO, *A Monte Carlo method for Poisson’s equation*, J. Comput. Phys., 90 (1990), pp. 123–140.
 - [14] S. DUO AND Y. ZHANG, *Computing the ground and first excited states of the fractional Schrödinger equation in an infinite potential well*, Commun. Comput. Phys., 18 (2015), pp. 321–350.
 - [15] ———, *Accurate numerical methods for two and three dimensional integral fractional Laplacian with applications*. Comput. Methods Appl. Mech. Engrg., 355 (2019), pp. 639–662.
 - [16] B. O. DYDA, A. KUZNETSOV, AND M. KWAŚNICKI, *Fractional Laplace operator and Meijer G-function*, Constr. Approx., 45 (2017), pp. 427–448.
 - [17] M. FAUSTMANN, M. KARKULIK, AND J. M. MELENK, *Local convergence of the FEM for the integral fractional Laplacian*, arXiv preprint arXiv:2005.14109, (2020).
 - [18] A. FRIEDMAN, *Stochastic differential equations and applications*. Vol. 2, Probability and Mathematical Statistics, Vol. 28, Academic Press [Harcourt Brace Jovanovich, Publishers], New York-London, 1976.
 - [19] M. GULIAN, M. RAISSI, P. PERDIKARIS, AND G. KARNIADAKIS, *Machine learning of space-fractional differential equations*, SIAM Journal on Scientific Computing, 41 (2019), pp. A2485–A2509.
 - [20] L. GUO, H. WU, X. YU, AND T. ZHOU, *Monte Carlo PINNs: deep learning approach for forward and inverse problems involving high dimensional fractional partial differential equations*, arXiv preprint arXiv:2203.08501, (2022).
 - [21] Z. HAO, H. LI, Z. ZHANG, AND Z. ZHANG, *Sharp error estimates of a spectral Galerkin method for a diffusion-reaction equation with integral fractional Laplacian on a disk*, Math. Comp., 90 (2021), pp. 2107–2135.
 - [22] Z. HAO AND Z. ZHANG, *Optimal regularity and error estimates of a spectral Galerkin method for fractional advection-diffusion-reaction equations*, SIAM J. Numer. Anal., 58 (2020), pp. 211–233.
 - [23] Z. HAO, Z. ZHANG, AND R. DU, *Fractional centered difference scheme for high-dimensional integral fractional Laplacian*, J. Comput. Phys., 424 (2021), p. 109851.
 - [24] A. E. KYPRIANOU, A. OSOJNIK, AND T. SHARDLOW, *Unbiased ‘walk-on-spheres’ Monte Carlo methods for the fractional Laplacian*, IMA J. Numer. Anal., 38 (2018), pp. 1550–1578.
 - [25] Z. MAO, Z. LI, AND G. E. KARNIADAKIS, *Nonlocal flocking dynamics: Learning the fractional order of PDEs from particle simulations*, Commun. Appl. Math. Comput., 1 (2019), pp. 579–619.
 - [26] Z. MAO AND J. SHEN, *Hermite spectral methods for fractional PDEs in unbounded domains*, SIAM J. Sci. Comput., 39 (2017), pp. A1928–A1950.
 - [27] R. METZLER AND J. KLAFTER, *The random walk’s guide to anomalous diffusion: a fractional dynamics approach*, Phys. Rep., 339 (2000), pp. 1–77.
 - [28] R. Metzler and J. Klafter, Joseph, *The restaurant at the end of the random walk: recent developments in the description of anomalous transport by fractional dynamics*, J. Phys. A, 37 (2004), p. R161.
 - [29] V. MINDEN AND L. YING, *A simple solver for the fractional Laplacian in multiple dimensions*, SIAM J. Sci. Comput., 42 (2020), pp. A878–A900.
 - [30] E. D. NEZZA, G. PALATUCCI, AND E. VALDINOCI, *Hitchhiker’s guide to the fractional Sobolev spaces*, Bull. Sci. Math., 136 (2012), pp. 521–573.
 - [31] G. PANG, L. LU, AND G. E. KARNIADAKIS, *fpinns: Fractional physics-informed neural networks*, SIAM Journal on Scientific Computing, 41 (2019), pp. A2603–A2626.
 - [32] G. PANG, M. D’ELIA, M. PARKS, AND G. KARNIADAKIS, *npinns: Nonlocal physics-informed neural networks for a parametrized nonlocal universal laplacian operator. algorithms and applications*, Journal of Computational Physics, 422 (2020), p. 109760.
 - [33] T. SHARDLOW, *A walk outside spheres for the fractional Laplacian: fields and first eigenvalue*, Math. Comp., 88 (2019), pp. 2767–2792.
 - [34] C. SHENG, J. SHEN, T. TANG, L.-L. WANG, AND H. YUAN, *Fast Fourier-like mapped Chebyshev spectral-Galerkin methods for PDEs with integral fractional Laplacian in unbounded domains*, SIAM J. Numer. Anal., 58 (2020), pp. 2435–2464.

- [35] M. SHLESINGER, B. WEST, AND J. KLAFTER, *Lévy dynamics of enhanced diffusion: Application to turbulence*, Phys. Rev. Lett., 58 (1987), p. 1100.
- [36] T. TANG, H. YUAN, AND T. ZHOU, *Hermite spectral collocation methods for fractional PDEs in unbounded domains*, Commun. Comput. Phys., 24 (2018), pp. 1143–1168.
- [37] H. YOU, Y. YU, M. D'ELIA, T. GAO, AND S. SILLING, *Nonlocal kernel network (NKN): a stable and resolution-independent deep neural network*, arXiv preprint arXiv:2201.02217, (2022).
- [38] E. C. ZACHMANOGLU AND D. W. THOE, *Introduction to partial differential equations with applications*, Dover Publications, Inc., New York, second ed., 1986.